A REDUCED COMPLEXITY GENERIC NOMA MAP RECEIVER FOR WIDEBAND MIMO CHANNELS

A THESIS SUBMITTED TO
THE GRADUATE SCHOOL OF NATURAL AND APPLIED SCIENCES
OF
MIDDLE EAST TECHNICAL UNIVERSITY

BY

HASAN AYKUT ŞATANA

IN PARTIAL FULFILLMENT OF THE REQUIREMENTS
FOR
THE DEGREE OF MASTER OF SCIENCE
IN
ELECTRICAL AND ELECTRONICS ENGINEERING

SEPTEMBER, 2020

Approval of the thesis:

A REDUCED COMPLEXITY GENERIC NOMA MAP RECEIVER FOR WIDEBAND MIMO CHANNELS

submitted by **HASAN AYKUT ŞATANA** in partial fulfillment of the requirements for the degree of **Master of Science in Electrical and Electronics Engineering Department, Middle East Technical University** by,

Prof. Dr. Halil Kalıpçılar
Dean, Graduate School of **Natural and Applied Sciences** _____

Prof. Dr. İlkay Ulusoy
Head of Department, **Electrical and Electronics Engineering** _____

Assist. Prof. Dr. Gökhan Muzaffer Güvensen
Supervisor, **Electrical and Electronics Engineering, METU** _____

Examining Committee Members:

Prof. Dr. Ali Özgür Yılmaz
Electrical and Electronics Engineering, METU _____

Assist. Prof. Dr. Gökhan Muzaffer Güvensen
Electrical and Electronics Engineering, METU _____

Prof. Dr. Elif Uysal
Electrical and Electronics Engineering, METU _____

Prof. Dr. Tolga Mete Duman
Electrical and Electronics Engineering, Bilkent University _____

Prof. Dr. Emre Aktaş
Electrical and Electronics Engineering, Hacettepe University _____

Date: 23.09.2020

I hereby declare that all information in this document has been obtained and presented in accordance with academic rules and ethical conduct. I also declare that, as required by these rules and conduct, I have fully cited and referenced all material and results that are not original to this work.

Name, Surname: Hasan Aykut Şatana

Signature :

ABSTRACT

A REDUCED COMPLEXITY GENERIC NOMA MAP RECEIVER FOR WIDEBAND MIMO CHANNELS

Şatana, Hasan Aykut
M.S., Department of Electrical and Electronics Engineering
Supervisor: Assist. Prof. Dr. Gökhan Muzaffer Güvensen

September 2020, 71 pages

Multiple input and multiple output (MIMO) technology and non-orthogonal multiple access (NOMA) are two important concepts for the next generation communication systems since they bring many advantages over conventional orthogonal systems. While there are numerous research over MIMO and power domain NOMA integration, the combination of MIMO and practical code domain NOMA schemes has not been investigated much in the literature, which is the subject of this thesis. In this study, we propose a generic maximum a posteriori (MAP) receiver based on the Ungerboeck observations from multiuser, where sparse code multiple access (SCMA) and multi-user shared access (MUSA) can be directly adapted. The proposed technique utilizes channel division multiple access (ChDMA) and code domain NOMA schemes on which a novel receiver architecture is structured at significantly reduced complexity. It outperforms conventional MMSE-SIC methods with very limited number of radio frequency (RF) chains and lower complexity. In addition, we provide an analysis in terms of bit-error rate and achievable information rate (AIR) showing mismatched decoding capacity under different code length and overloading scenarios for

uplink transmission where flexible structure of MUSA is exploited.

Keywords: NOMA, MIMO, Equalization, Multi-User Detection, MUSA, SCMA

ÖZ

GENİŞ BANTLI ÇOKLU GİRİŞ ÇOKLU ÇIKIŞ KANALLAR İÇİN DÜŞÜK KARMAŞIKLIKLI NOMA MAP ALICISI

Şatana, Hasan Aykut
Yüksek Lisans, Elektrik ve Elektronik Mühendisliği Bölümü
Tez Yöneticisi: Dr. Öğr. Üyesi. Gökhan Muzaffer Güvensen

Eylül 2020, 71 sayfa

Çoklu giriş ve çoklu çıkış (MIMO) teknolojisi ve ortogonal olmayan çoklu erişim (NOMA), geleneksel sistemlere göre birçok avantaj sağladıkları için gelecekteki kablosuz sistemler için çok önemli yöntemlerdir. Güç alanı NOMA yöntemleri ile yoğun MIMO sistemleri üzerine araştırmalar mevcutken, bu tezin konusu olan pratik kod alanında NOMA şemalarının yoğun MIMO ile entegrasyonu konusunda çok az çalışma vardır. Bu tezde, seyrek kodlu çoklu erişim (SCMA) ve çok kullanıcılı paylaşımlı erişimin (MUSA) doğrudan uyarlanabildiği çok kullanıcılı Ungerboeck gözlemlerine dayalı genel bir maksimum artçıl kestirimli (MAP) alıcı öneriyoruz. Önerilen teknik ile kod alanındaki dizin modülasyonunu ve kanal bölmeli çoklu erişim (ChDMA) yöntemleri önemli ölçüde azaltılmış karmaşıklıklı yeni bir alıcı mimarisinde birleştirilmiştir. Önerilen yöntem sınırlı sayıda radyo frekansı (RF) zincirleri ile ve daha düşük karmaşıklıkla geleneksel MMSE-SIC yöntemlerinden daha iyi performans gösterir. Ayrıca bu çalışmada, MUSA'nın esnek yapısı kullanılarak farklı kod uzunluğu ve aşırı yükleme senaryoları altında uyumsuz kod çözme kapasitesini gösteren ulaşılabilir bilgi hızı (AIR) ve bit hata oranı açısından analizler gösterilmiştir.

Anahtar Kelimeler: Dikgen Olmayan Çoklu Erişim, Çoklu Giriş ve Çoklu Çıkış, Çoklu-Kullanıcı Kestirimi, MUSA, SCMA

To My Family..

ACKNOWLEDGMENTS

I would like to express my appreciation to my supervisor Assoc. Prof. Gökhan M. Güvensen for his supervision and endless support throughout this three-year journey. His positive attitude, thoughts, and constant motivation always inspired me to work at my best. I would like to thank him for giving this opportunity.

My special thanks to ASELSAN A.Ş. for the full graduate study supports. They provide not only time but also hardware and processing power for my graduate studies. I would also like to thank Soner Yeşil, Burak Gürtunca, Cansu Şen and Altuğ Kaya who are my colleagues at ASELSAN.

I want to thank to my family members Günay Şatana, Demet Şatana and Hakan Fevzi Şatana for giving me unconditional support during my whole life and the thesis period.

I am also deeply thankful to Ayşe Rana Bal, Eda Begüm Berberoğlu, Utku Gülgeç, Hüseyin Tunç Bilgiç for their encouragements and supports during my whole studies.

TABLE OF CONTENTS

LIST OF TABLES

TABLES

LIST OF FIGURES

FIGURES

LIST OF ABBREVIATIONS

ABBREVIATIONS	
AIR	Achievable Information Rate
APP	A Posteriori Probability
BER	Bir Error Rate
CCM	Code Correlation Metric
CDMA	Code Division Multiple Access
CMF	Channel Matched Filtering
FDMA	Frequency Division Multiple Access
FG	Factor Graph
GMI	Generalized Mutual Information
IoT	Internet of Things
ISI	Inter Symbol Interference
MA	Multiple Access
MAC	Multiple Access Channel
MAP	Maximum a-posteriori Probability
MIMO	Multiple Input Multiple Output
MF	Matched Filter
ML	Maximum Likelihood
MLSE	Maximum Likelihood Sequence Estimation
MMSE	Minimum Mean Square Error
MPA	Message Passing Algorithm
MUSA	Multi-User Shared Access
MTC	Machine Type Communication
MUD	Multi User Detection

MUI	Multi-User Interference
NOMA	Non-Orthogonal Multiple Access
OFDMA	Orthogonal Frequency Division Multiple Access
OMA	Orthogonal Multiple Access
RE	Resource Element
SC	Single Carrier
SCMA	Space Code Multiple Access
SIC	Successive Interference Cancellation
SINR	Signal-to-Interference-plus-Noise Ratio
SPA	Sum-Product Algorithm
TDMA	Time Division Multiple Access
UCM	Ungerboeck Correlation Metric
UMPA-BDF	Ungerboeck Type Message Passing Algorithm
WGN	White Gaussian Noise

NOMENCLATURE

Scalars

N_c Codeword length

L_c Number of channel taps

M Alphabet size

L Effective channel length

K Number of user in a MAC

N Number of antennas (RF Chains) in receiver

I_k^u At symbol time k NOMA waveform/codeword index of u^{th} user

N_0 AWGN Noise Power

E_s Average symbol energy

$x^{(u)}[n]$ Upsampled baseband equivalent of the transmitted signal of u^{th} user

Vectors

$\mathbf{y}[n]$ Received upsampled NOMA signal from multiple antennas

$\mathbf{h}^{(u)}[n]$ Baseband equivalent response quasi-static MIMO channels of u^{th} user, containing the multipath components

$\mathbf{r}^{(u)}[k]$ At symbol time k, CMF and code MF outputs of u^{th}

$\mathbf{c}^{(v)}[k]$ At symbol time k, equivalent codeword index of codebook for v^{th} user

$\mathbf{v}^{(u)}[k]$ At symbol time k, correlated noise vector sequence of u^{th} user

Matrices

$\mathbf{G}_{m_1,m_2}^{(u_1,u_2)}[k]$ Code correlation metric for m_1^{th} waveform of user u_1 and m_2^{th} waveform of user u_2

$\mathbf{I}$ Identity Matrix

$\mathbf{W}$ MMSE filter coefficient matrix

$\mathbf{G}_{mmse}$ MMSE filter correlation matrix

$\mathbf{R}^{(u,v)}[l]$ Ungerboeck Correlation Metric Matrix

CHAPTER 1

INTRODUCTION

1.1 Motivation

In this thesis, we will focus mostly on the multiple access (MA) concept and multi-user detection (MUD) with reduced complexity receivers in cellular networks which explains how millions of subscribers are served by telecommunication operators simultaneously. Combining multiple signals coming from each user and transmitting them over a common channel is known as multiplexing. When multiplexing is used to allow multiple users to communicate over a single common channel and share a finite amount of radio spectrum simultaneously, it is called multiple access. There are two types of MA channels: first are uplink channels which correspond to a multiple transmitter to one receiver structure and are also the main interests throughout this thesis, and second are donwlink channels which correspond to a single transmitter to multiple receiver structure.

Telecommunication systems have employed several ways to share a finite spectrum resource among users in frequency, time or code domain from the first generation (1G) to fifth generation (5G), and MA has been the key technology to distinguish different wireless systems. For more than 80 years, various methods have been created and tested for MA schemes in communication to use the spectrum efficiently. As a result of the studies, techniques such as, frequency-division multiple access (FDMA), time-division multiple access (TDMA), code-division multiple access (CDMA), and orthogonal frequency-division multiple access (OFDMA) has been developed. In these conventional multiple access schemes, except for CDMA, different users are allocated to orthogonal resources in either the time, frequency, or code domain in or-

der to avoid inter-user interference, making signal and message detection relatively simple. However, these orthogonal multiple access (OMA) methods can only support a limited numbers of users due to limitations in the numbers of orthogonal resource blocks, which limits the spectral efficiency and the capacity of current networks [3]. Considering the internet of things (IoT), machine-type communication (MTC), and mobile Internet requirements, spectral efficiency becomes one of the key challenges handling such data traffic [4, 8, 9]. Additionally, massive connectivity, low latency, and short packet duration are needed for 5G communication. Recently, Non Orthogonal Multiple Access (NOMA) has been investigated to deal with the problems of OMA. Unlike conventional OMA methods, NOMA uses non-orthogonal physical resources such as time and frequency where overloading can be realized. Therefore, NOMA can support more users as 5G networks require by fully utilizing the limited spectrum resources. However, this process creates extra interferences due to the non-orthogonality among resources, requiring more complex receiver structures. [8]

NOMA schemes were initially introduced for single-antenna systems and their extension to multiple input multiple output (MIMO) systems is nowadays an important research direction. In addition, low-complexity interference cancellation algorithms should be developed so that NOMA schemes become more practical. The high complexity of the message passing algorithm (MPA) and the error propagation of the successive interference cancellation (SIC) are the two main problems of current receiver architectures. Conventional and advanced receivers for some NOMA schemes are described in [10] and references therein. Factor graph based iterative receivers for a downlink MIMO-SCMA system with cooperation is proposed and performance comparison with existing receivers is provided where the number of antennas is equal to number of physical resources in [11]. Overloaded and coded massive MIMO-NOMA systems and capacity-achieving low-complexity Linear Minimum Mean Square Error (LMMSE) detection based receivers are studied in [12, 13]. A Gaussian message passing algorithm is proposed for overloaded massive MIMO system in [14]. In [15], beamspace MIMO at mm-wave bands is integrated with Sparse Code Multiple Access (SCMA), which is one of the popular NOMA schemes in code domain, where the number of RF chains is equal to the number of physical resources.

Although there are some efforts to combine NOMA with MIMO systems, there is a

lack of literature for the adaptation of some practical NOMA schemes such as multi-user shared access (MUSA) to MIMO architecture employing single-carrier in wide-band mm-wave channels. Code domain NOMA schemes are generally considered with multicarrier transmission since inter-symbol interference (ISI), which is a signal distortion due to the other sent symbols is a serious problem for single carrier (SC) systems [4, 9] and low complexity receivers considering the ISI mitigation for single carrier systems have not been proposed yet. That is, most of the existing researches for massive MIMO systems adopt a flat-fading channel model by considering the use of orthogonal frequency division multiplexing (OFDM) [16].

A generic low complexity receiver design for fifth-generation (5G) NOMA wireless networks and beyond are cutting-edge research topics that motivate a very wide range of research problems [3]. In the light of these motivations, in this thesis we provide a generic unification of practical code domain NOMA schemes which are SCMA and MUSA and MIMO architecture with a reduced complexity MUD receiver implementation where the number of antenna elements/RF chains is limited.

1.2 Multiple Access Concept from 1G to 4G

1.2.1 First Generation (1G) with Frequency Division Multiple Access (FDMA)

1G was officially introduced in 1982 by Bell Labs, and it was popularly known as the Advanced Mobile Phone System (AMPS) [1]. Here, the key idea was to divide geographical areas into cells and implement frequency reuse to serve each cell with a base station. That is, since the transmitted signal power falls off with distance, with 1G two users can operate on the same frequency at separate cells with very low interferences.

The technology used was analog frequency modulation (FM), and the spectrum was divided firstly into 30 kHz then reduced to 10 kHz segments, called channels which utilized the entire bandwidth for a single user. First generation analog systems used FDMA to provide each user a duplex channel. FDMA which uses frequency division multiplexing, provides chunks of the frequency spectrum to each user for data

transmission. Guard bands are introduced to avoid any interference due to imperfect filtering, adjacent channel interference and Doppler effects. An illustration of FDMA channels is given in Figure 1.1.

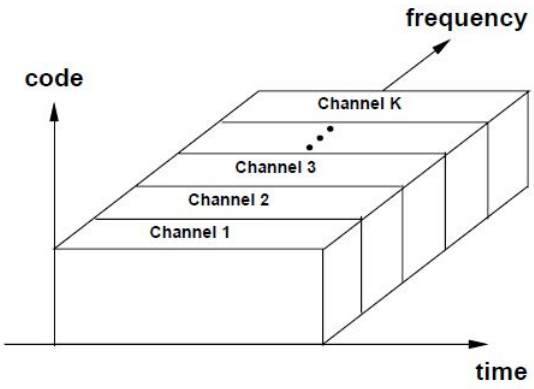

Figure 1.1: Frequency-Division Multiple Access [1]

1.2.2 Second Generation (2G) with Time Division Multiple Access (TDMA)

Second generation (2G) cellular telecom networks were commercially launched in 1991 in Finland by the European Telecommunications Standards Institute (ETSI) based on Global System for Mobile Communications (GSM) standards. The key difference from 1G is the shift from analog to digital communication enabling better quality voice communication via voice coders, supports of data services, data security and increased system capacity. 2G introduced data services for mobile, starting with SMS text message. During these times, Internet was becoming popular and transfer of data was becoming more of a prevalent issue, therefore, in the later release of 2G which are General Packet Radio Service (GPRS) and Enhanced Data Rates for GSM Evolution (EDGE) mobile phones started supporting web browsing as the multimedia services with up to 500 Kbps data rate with digital GMSK and 8PSK modulations. [1]

In 2G, in order to increase system capacity, along with the frequency band division into channels, time also was divided into slots using TDMA. TDMA uses time division multiplexing which allows multiple users to share a common frequency band by allocating different non overlapping cyclically-repeating time slots which are orthogonal in signaling dimension, as shown in Figure 1.2. These TDMA channels use the

whole system bandwidth, called a wideband system. Hence, some form of ISI mitigation is required. In TDMA, due to the cyclically-repeating structure, transmission is not continuous for users. Unlike FDMA, in TDMA it is possible to assign multiple channels to a single user, however, synchronization among the different users to maintain orthogonality is required. Multipath, can also destroy time-division orthogonality, significantly reducing the system capacity [3]. Apart from these, in TDMA, receiver complexity is exponential according to the modulation scheme, constellation size , and number of antennas involved. [1]

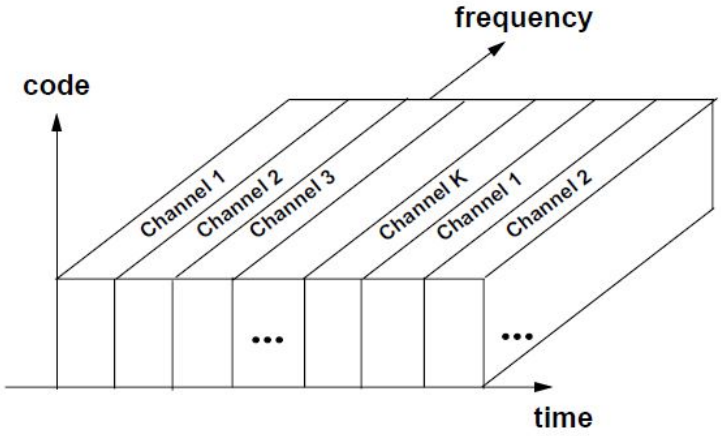

Figure 1.2: Time-Division Multiple Access [1]

1.2.3 Third Generation (3G) with Code Division Multiple Access (CDMA)

After EDGE was successfully implemented, the creation of such a large and complex system specifications required a well-structured organization. This gave birth to 3GPP and which determines the standards that can maintain the requirement for radio technology and effective use of the spectrum. The international telecommunications union (ITU) provided 3G goals, and the 3GPP standards created specifications to support implementations which satisfied these requirements. With this generation, users are provided the ability to surf the Internet and have simultaneous voice and data services. According to 3GPP standards, 3G uses QPSK, 16QAM and 64 QAM digital modulations in time division duplexing (TDD) or frequency division duplexing (FDD) modes with 5 MHz bandwidth,and data rates up to 1 Mbps. In the later releases, utilizing downlink MIMO operation with higher order modulations 3G pro-

vides data rates up to 28 Mbps for the downlink and 11 Mbps for the uplink. [3]

In 3G, the MA technique shifted from using TDMA to CDMA, which later evolved into Wideband CDMA (WCDMA) [1]. CDMA which is based on code division multiplexing is a technique in which the data bits are modulated by a high frequency orthogonal or non-orthogonal sequence of bits to spread the signals over a large frequency band as illustrated in Figure 1.3 , and multiple such signals from different users are then transmitted over the same frequency as in Figure 1.4. In order to retrieve the signal, the receiver must have the same spreading sequence, which is multiplied to this composite signal in a process called despreading. In the downlink, orthogonal spreading codes such as Walsh codes are used although the orthogonality can be degraded by multipath. As for uplinks, non-orthogonal codes are preferred due to the difficulty of user synchronization and the complexity of maintaining code orthogonality with multipath, as a result, less efforts are required for user coordination in time and frequency. In addition, non-orthonality in uplinks remove the hard limit which restrict the number of channels, that is there is no need to search for orthogonality between channels. However, non-orthogonal codes cause mutual interference between users since the system bandwidth is shared among more users at the same time with non-orthogonal codes, which reduces the performance of all the users. [3]

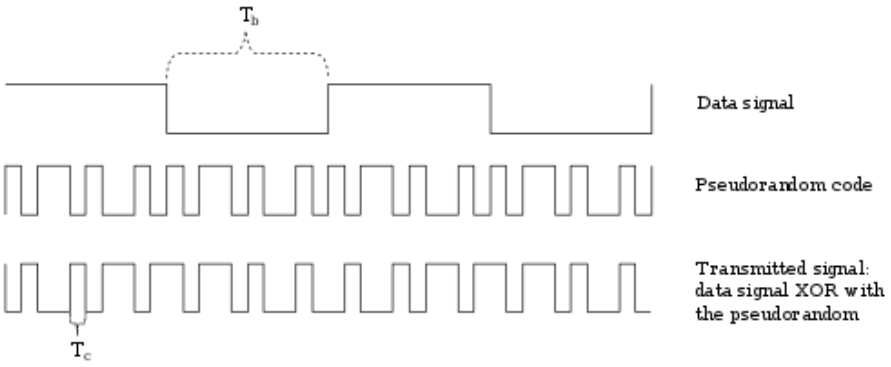

Figure 1.3: Generation of CDMA [2]

A non-orthogonal CDMA scheme also suffers from near-far effect, which must be compensated with power control mechanism. The near-far effect arises in the uplink because the channel gain between a user's transmitter and the base station's receiver is different for different users. For example, considering two users, one is close to the BS and the other is far away: If both users transmit at the same power level,

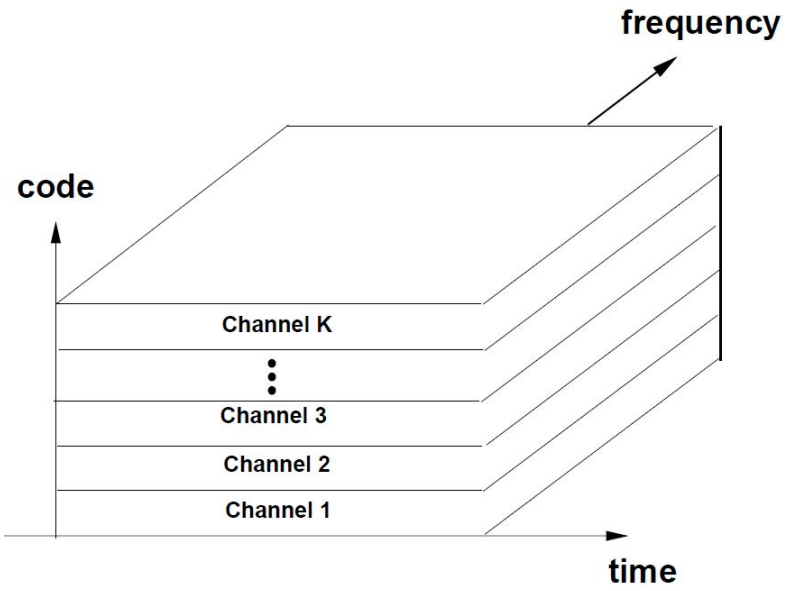

Figure 1.4: Code-Division Multiple Access [1]

the signals from far user is lost in close user's signal. Therefore, power control is implemented in order to make all users' signal power roughly equal at the receiver so that fading effects are gone and the near-far problem can be eliminated [3].

CDMA with non-orthogonal spreading codes can also use MUD to reduce interference between users [1], since MUD provides significant performance improvements even under perfect power control. An example of MUD is a rake receiver, which is used for the reception of WCDMA signals and is, designed to counter the effects of multipath fading with time diversity. Also, in CDMA systems, receiver complexity grows linearly with data rate, modulation scheme used, and number of antennas supported [3].

CDMA evolution reached to its limits and it could not be developed further even when the higher order modulations and MIMO was used for spatial multiplexing to increase the data rate within an allowed spectral bandwidth. Additionally carrier aggregation methods were tried, which increased the spectral bandwidth, but still spectral efficiency remained unchanged. Unfortunately, signal spreading operation which causes bandwidth expansion, and not being able to reach the desired high data rates prohibited the evolution of WCDMA system any further.

1.2.4 Fourth Generation with Orthogonal Frequency Division Multiple Access (OFDMA)

The fourth generation (4G) was created to support exponential system capacity and data rate needs since much higher rates were required to allow mobile Internet access with video applications. At this point in the cellular evolution, the industry converged to a single standard, Long Time Evolution (LTE) . The LTE cellular system is based on OFDMA. The frequency bandwidth options have been expanded to 1.4, 3, 5, 10, 15, and 20 MHz for flexible bandwidth formation [3]. OFDMA uses FDMA technique via inverse fast Fourier Transform (IFFT and FFT) operations where the divided frequencies are 15 kHz apart. Each frequency channel is called a subcarrier, and in OFDMA it is required to keep the spacing between subcarriers less than the coherence bandwidth of the wireless channel, unlike CDMA. As a result of this selection, each subcarrier sees a flat frequency response at the receiver, which enables the receiver to make frequency domain equalization and hence mitigate the flat channel effects of transmission. In other words, the receiver does not have to deal with complex time domain equalization techniques as in TDMA while using the OFDMA, making it an attractive option for multipath ISI channels.

A block diagram providing an example of the OFDMA waveform generation is provided in Figure 1.5. Some of the important points related to the OFDMA method are the following: firstly the number of subcarrier directly affects the data rate, user capacity, and occupied bandwidth in the system. Secondly, it is desired to have large number of subcarriers while keeping occupied bandwidth under control using the spectral shaping function. In addition, OFDM symbols pretty much suffer from peak to average power ratio (PAPR), causing vulnerability against power amplifier nonlinearities and loss of average transmitted power. Lastly, in order to make a frequency domain signal processing with FFT with OFDM transmission, circular convolution needs must be satisfied with the cyclic prefix (CP) which contains the multipath components of the wireless channel. This CP duration must be long enough to contains all corresponding multipaths.

Some methods from 3G cellular system like MIMO and higher order modulations shows their benefits more in the OFDMA for increasing data rates, as a result, MIMO

support is needed to accommodate multiple layers through spatial multiplexing with large constellations in OFDMA.

In OFDMA, users are multiplexed in both the frequency and time domains, as shown in Figure 1.6 for LTE system. A unit of allocation is called resource block RB. A RB consist of 12subcarriers by 7 OFDM symbols which is equal to 84 OFDM symbols. Some of these modulation symbols can be used as pilot for channel estimation instead of data symbols. Each RB contains 12 x 15 = 180kHz of bandwidth. In the figure, assuming QPSK modulation, there are four different symbols represented by four different colors. Each color represents one resource element (RE) and carries two bits with QPSK modulation.

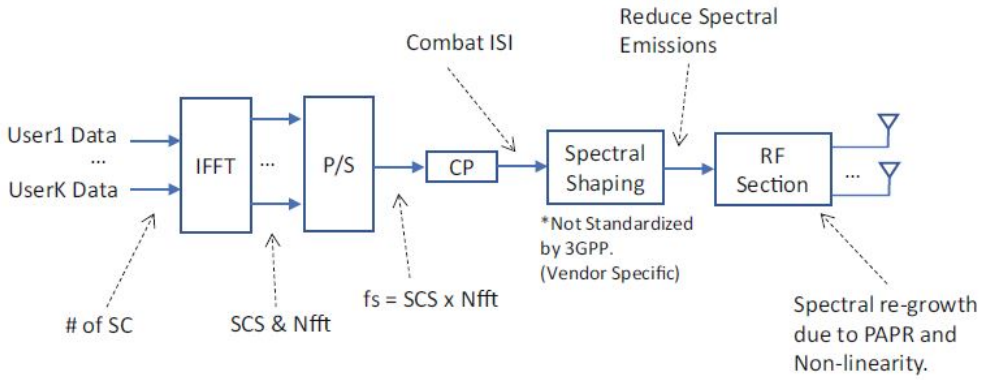

Figure 1.5: OFDMA waveform generation with K sub-carrier (SC) [3]

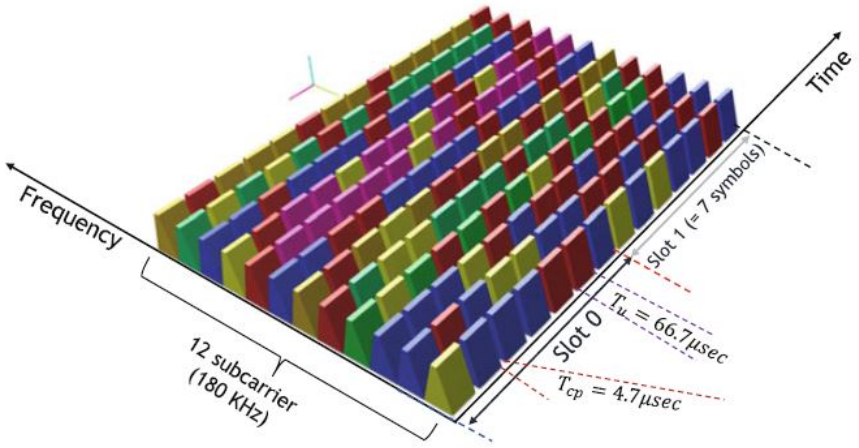

Figure 1.6: Time/frequency representation of the OFDM signal for LTE standard. There are four different symbols (QPSK) each represented by one color [3]

There are important disadvantages with OFDM that affect the efficiency of the systems, such as:

- CP overhead: The need for adding the CP introduces redundancy and loss of spectral efficiency.
- Sensitivity to frequency and timing offsets: Keeping the orthogonality between subcarriers requires the transmitter and receiver to have the exact same reference frequency. Any offset can brake the orthogonality and cause inter-carrier interference (ICI)
- High out-of-band (OOB) emission: Due to the sinc pulses in frequency domain, OFDM requires infinite bandwidth if there is no spectral shaping control.
- High peak-to-average power ratio (PAPR): PAPR is the result of summation of sinusoid in the IFFT process, the envelope of the OFDM waveform has a large variation which result in clipping problems when the signal passes through non-linear device like a power amplifier.

1.3 Next Generation Multiple Access Technique Non Orthogonal Multiple Access Concept (NOMA)

Due to flat fading advantages and for backward compatibility reasons, OFDM will still be the main waveform for 5G systems with some modifications. Especially CP overhead and OOB emission issues are widely reconsidered in the 5G systems, with candidates like Filtered OFDM (F-OFDM), Windowed OFDM (also known as weighted overlap and add or WOLA-OFDM), Universal Filtered OFDM (UF-OFDM) and Filter Bank Multi-Carrier (FBMC). However, along with the traditional OMA structures, NOMA techniques are intensive research subject for the next generations due to massive connectivity advantages as indicated by 3GPP Release-16 [3].

The key idea behind NOMA is to serve multiple users in the same resource block, such as a time slot, subcarrier, or spreading code [17]. Considering OFDMA, a RB cannot be allocated to more that one user, since the user's signal must be orthogonal in frequency or time. On the contrary, NOMA allows multiple users to share same

RE which can be in time, frequency, space or time. In other words, in OMA the number of users that can be supported is then limited by the number of orthogonal resources available while NOMA admits and utilize intra-cell interference in the resource allocation of users. Therefore, interference cancellation techniques such as success interference cancellation (SIC) or multi-user detection (MUD) are used to mitigate this interference [17].

The next generation of wireless networks must support very high throughput, low latency, and massive connectivity. In terms of massive connectivity, NOMA theoretically can serve an arbitrary number of users even within one resource block by superimposing the signals, therefore, NOMA can be a great candidate to IoT applications where a large number of devices randomly transmit a small number of packets. As for low latency requirements: with OMA, any device has to wait until an occupied RB to becomes available while NOMA supports flexible scheduling since it can accommodate variable number of users. From the point of spectral efficiency, NOMA is the theoretically optimal way of using the spectrum for both uplink and downlink communications in a single-cell network since NOMA users can enjoy the whole bandwidth while the OMA users are limited to a smaller fraction [3].

In the information theoretical perspective, the capacity of MAC under AWGN and fading channels with NOMA based techniques result in superior rate region as compared to OMA versions, which is valid for all NOMA and OMA schemes [4]. Capacity analysis are generally presented for two users in the literature, however, it is given in [4] that the results for the simple two-user case can be extended to the general case of an arbitrary number of users. Channel capacity analysis comparison for NOMA and OMA is given in Figure 1.7 for uplink two user scenario where p_i represent user signal power h_i shows the channel of i^{th} user and $i = 1, 2$. From the figure, it is observed that uplink NOMA can achieve the capacity region while OMA is sub-optimum in general except for one point where the user rate-fairness cannot be maintained.

Although NOMA is a known and accepted technique, there is an arising dispute on the definition of "non-orthogonality". Throughout this thesis, we consider NOMA in terms of overloading viewpoint, meaning having more than one user per available

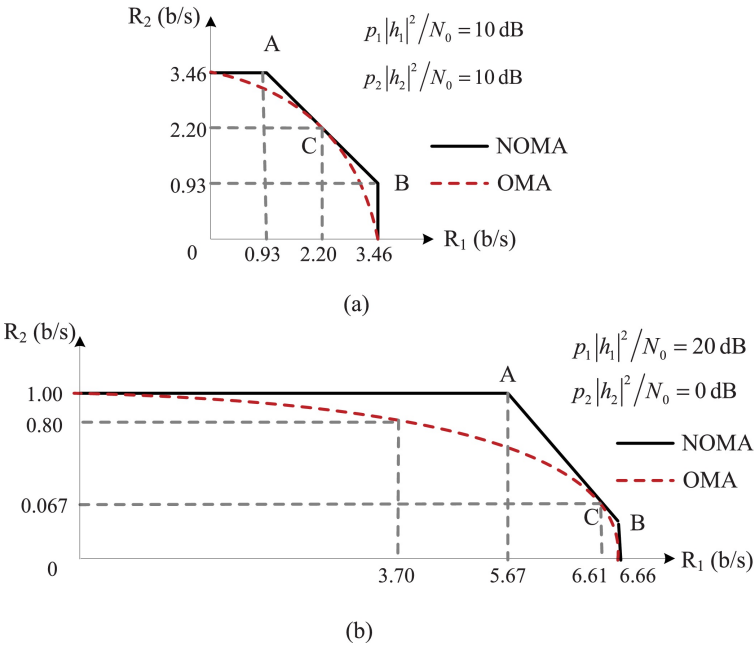

Figure 1.7: Channel capacity comparison of OMA and NOMA for uplink AWGN channel (a) shows Symetric channel ; (b) Asymmetric channel [4]

resource element in the time, frequency, code, or space domain. With this definition, a CDMA system can be seen as a NOMA scheme if it is overloaded. Examples of this overloading viewpoint are generally defined as code domain NOMA schemes such as, low density spreading (LDS), LDS-OFDM, SCMA and MUSA. Additionally, by this viewpoint, the number of receiver antennas have to be less than the number of users in a MAC since antennas can be considered as new signaling dimensions to assign users. Therefore, in this thesis, we are focusing on the uplink MIMO MAC where the number of RF chains is limited in the receiver.

A brief classification for OMA and NOMA schemes can be seen in Figure 1.8. NOMA schemes can be realized mainly in two domains which are power domain NOMA or code domain NOMA.

1.3.1 NOMA in the Power Domain

Power domain NOMA exploits the channel strength differences between users in same resource block where detection is based on different power levels rather than different frequency or time blocks, and therefore it is the optimal capacity-achieving

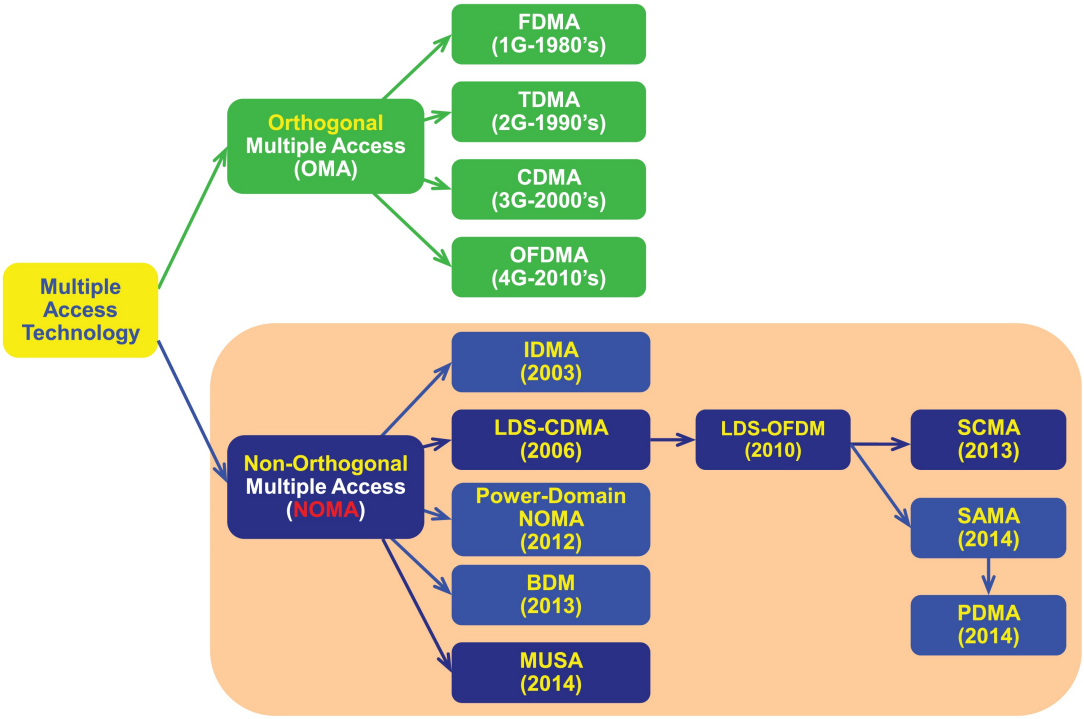

Figure 1.8: Multiple Access Schemes Brief Classification [4]

MA technique in a single-cell network. The spectrum and power allocation for power domain NOMA is graphically compared with that of OMA in Figure 1.9. Since users are separated in power rather than frequency, instead of multi-carrier modulation techniques, single carrier modulation types are preferred for power domain NOMA.

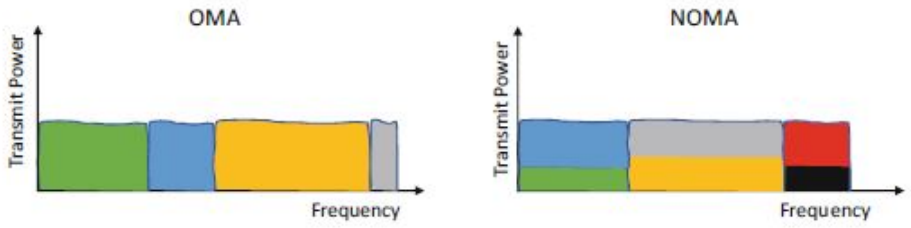

Figure 1.9: OMA and NOMA power and spectral allocations [3]

Knowing that OMA is strictly suboptimal, to be specific, the capacity region is achieved by point-to-point codes, successive cancellation decoding, and time-sharing. Considering a K user MAC, the users transmit their signals concurrently and the base station applies Succesive Interference Cancallation (SIC) decoding. Dual case is valid in broadcasting where the user equipment's receiver first decodes the strongest user's signal then removes them from received signals. Based on information theory,

non-orthogonal multiplexing using superposition coding at the transmitter and using SIC at the receiver is the optimum from the perspective of achieving the capacity region [4].

Due to the some practical issues like power allocation to the users, signaling overhead, error propagation in SIC, to achieve further improvements power domain NOMA and MIMO combination is studied much in the literature. Apart from the superiority of MIMO-NOMA over MIMO-OMA techniques in terms of capacity, in the realistic hardware setups the cell throughput of MIMO-NOMA with power domain is $\%30$ higher as compared to MIMO-OFDMA solutions [4]. However, most of the analysis work on power domain NOMA is limited to single-cell analysis [3]. Particularly, as wireless networks get crowded, inter-cell interference (ICI) becomes a major problem, which might reduce the advantages of power domain NOMA.

1.3.2 NOMA in Code and Other Domains

Code-domain NOMA assigns non-orthogonal codes to the each user within the same time-frequency resource block, supporting overloaded transmission. It is a trade-off between system performance and the receiver complexity, and has a spreading and shaping gain with the cost of extra signal bandwidth in comparison with power-domain NOMA [3]. Code-domain NOMA is known as the multi-carrier NOMA since there is not any receiver that offers ISI equalization with a reasonable complexity with the single-carrier solutions, which is the topic of this thesis work.

The code domain NOMA concept came from the classical CDMA systems. Unlike CDMA, spreading sequences are restricted to sparse or low cross-correlation short sequences in code domain NOMA where higher overloading scenarios can be realized. Code domain NOMA schemes and the improvements can be followed from the Figure 1.8. Initial form of code domain NOMA structures based on the low density spreading (LDS) which is extended later to LDS-CDMA in [18] and LDS-OFDMA in [19]. LDS-CDMA is based on sparse spreading sequences together with low complexity MUD based decoding whereas the LDS-OFDM exploits all of OFDM advantages that removes the ISI. LDS methods are designed to limit the amount of interference between users in chip level. An important extension of the LDS-CDMA method

is SCMA in [20] which shows better performance still keeping the lower complexity. Another improved extension forms of the CDMA is Successive interference cancellation amenable multiple access (SAMA) in [21] and MUSA in [22] which utilizes specifically designed short spreading sequences with SIC based receivers.

Apart from the power domain and code domain NOMA schemes, there are also different types of NOMA schemes. One example can be the Spatial Division Multiple Access (SDMA) in [23] where combination of classical CDMA spreading sequences and unique channel impulse responses of each user is utilized to distinguish users. Therefore, SDMA enables robust NOMA transmission against ISI in dispersive channels. However, SDMA requires accurate channel information which might be difficult to provide for most of the scenarios. Due to this reason, SDMA needs joint iterative channel and data estimation algorithm for the MUD designs. Another example of this class is the pattern division multiple access (PDMA) in [24] which exploits non-orthogonal patterns designed to minimize correlation among users while maximizing the diversity. In PDMA, multiplexing can be done in code, power or spatial domains. Third example of this class of NOMA is Signature-Based NOMA scheme (S-NOMA) in [25]. In this scheme, data or bits of each users are multiplexed with the help of specific signature pattern. As a fourth class interleave-grid multiple access (IGMA) [26] can be given where users are differentiated by different grid mapping patterns. There are also another NOMA schemes such as spreading based non orthogonal coding multiple access (NCMA), bit division multiple access (BDM) where users are partitioned in bit levels [4] and compressive sensing based NOMA methods in [4]

Among all the NOMA schemes, two promising code domain NOMA schemes which are SCMA and MUSA becomes more popular due to their capacity achieving performances with low complexity transmitter and receiver designs. In this thesis, for all the performance measurements of the proposed receiver architecture, we will employ these two schemes. In the following sections SCMA and MUSA will be investigated in a more detailed way.

1.3.2.1 Sparse Code Multiple Access (SCMA)

SCMA is based on the non-orthogonal spreading technique where the multi-dimensional QAM symbol modulation and spreading are combined together. Shaping gain stemmed from multi-dimensional constellation is the main performance improvements against low density spreading (LDS) [20, 27]. In SCMA, different users have different codebooks via sparsity in codewords. Utilizing sparsity of codewords allows comparably low complexity MUD based MPA at the receiver since each resource element (RE) in codewords are shared among a subset of active users. The sparsity of the signal provides a small collision of users' data reducing the Multi-user interference at the receiver side which is based on chip rate processing.

SCMA decoder can be defined as $f : \mathbb{B}^{log_2(M)} \rightarrow \mathbf{X}$, $\mathbf{x} = f(\mathbf{b})$ where $\mathbf{X} \subset \mathbb{C}^{N_c}$ with cardinality $|\mathbf{X}| = M$. x is an sparse N_c dimensional complex codeword. That is, SCMA encoder is $f := \mathbf{V}g$ where binary mapping matrix $\mathbf{V} \in B^{K \times N_c}$ with $N_c - d$ all zero rows so that after eliminating them identity matrix $\mathbf{I}_{N_c}$ is remained. Resulting codebook includes M codewords and each consist of N_c complex values with d non-zero elements that comes from a multi-dimensional constellations [27].

Figure 1.10 shows an example of codebooks for transmitting $K = 6$ users that are identified as the data layers. In this example figure, each of the codebook has 8 multi-dimensional complex codewords from Figure 1.11. The length of codewords $N_c = 4$ for this example scheme. While transmitting, the codeword of each user/layer is selected based on the input bit sequence. The overloading factor can be expressed as K/N_c for the SCMA based transmissions.

Current SCMA system requires a reduced complexity receiver independent from the cardinality size, optimum codebook design, optimum multi-constellation design and flexibility for different overloading scenarios for future works [3].

Although current SCMA designs are always used with OFDM modulation in order not to deal with the complex ISI problem at the receiver during message passing, in this thesis, with the proposed UMPA-BDF receiver design allows usage of single carrier system with lower complexities.

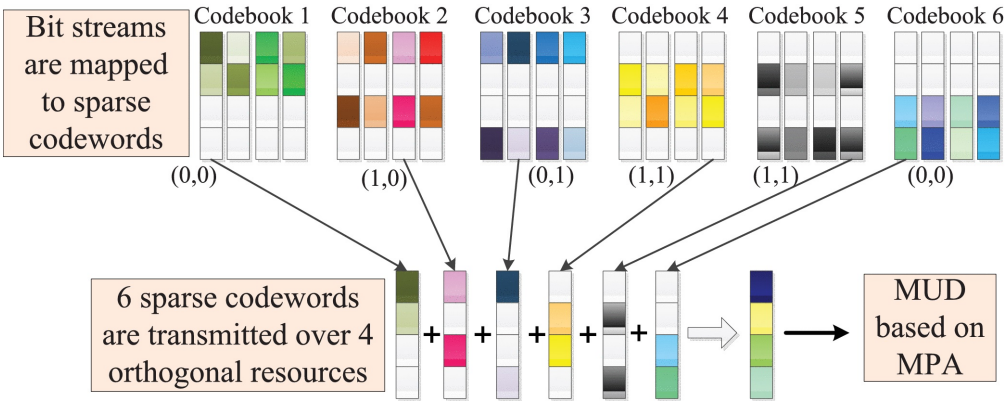

Figure 1.10: SCMA codebook bit-to-codeword mapping. [5]

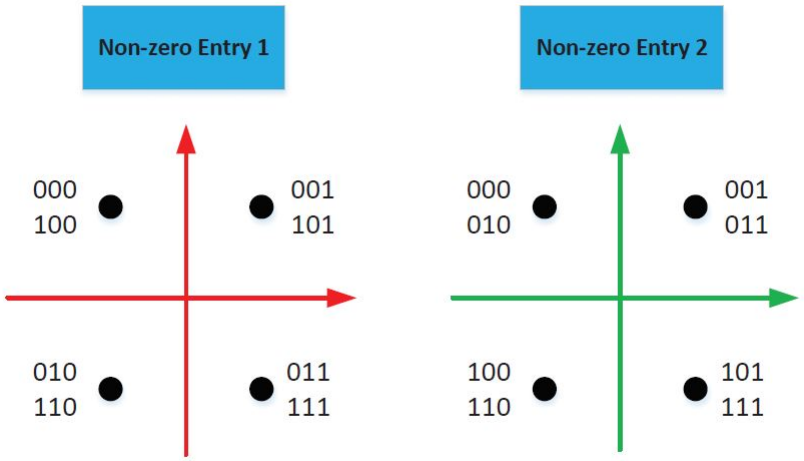

Figure 1.11: Example of SCMA 8-point codebook [5]

1.3.2.2 Multi-User Shared Access (MUSA)

MUSA is a code domain NOMA scheme, which can be regarded as the improved version of CDMA [22]. Unlike CDMA, MUSA can employ overloading via non-orthogonal low correlation complex spreading sequences at transmitter [28], as a result, it is an important candidate to support massive connectivity that 5G demands considering the potential scalability issues of SCMA.

MUSA provides grant-free access where each user can select the spreading code autonomously, eliminating the need of resource coordination by base station. Therefore, it minimizes signaling overhead and power consumption at the same time [22].

In the Figure 1.12, the transmitter and receiver structure of the NOMA with MUSA scheme can be seen for K simultaneous users. Fig.1 shows the transmitter and receiver structure of the MA scheme with K simultaneous users.The databits d_k of user k are encoded generating the coded bits c_k. Then the c_k is modulated with x-QAM modulator where x is the constellation size producing m_k. Now, m_k is spread by a complex spreading code s_k of short length N_c. On the receiver side, successive interference cancellation (SIC) is used to decode the data bits of K simultaneous users from the received superimposed signal. Overloading factor for the MUSA is K/N_c where N_c is flexible different than the SCMA scheme.

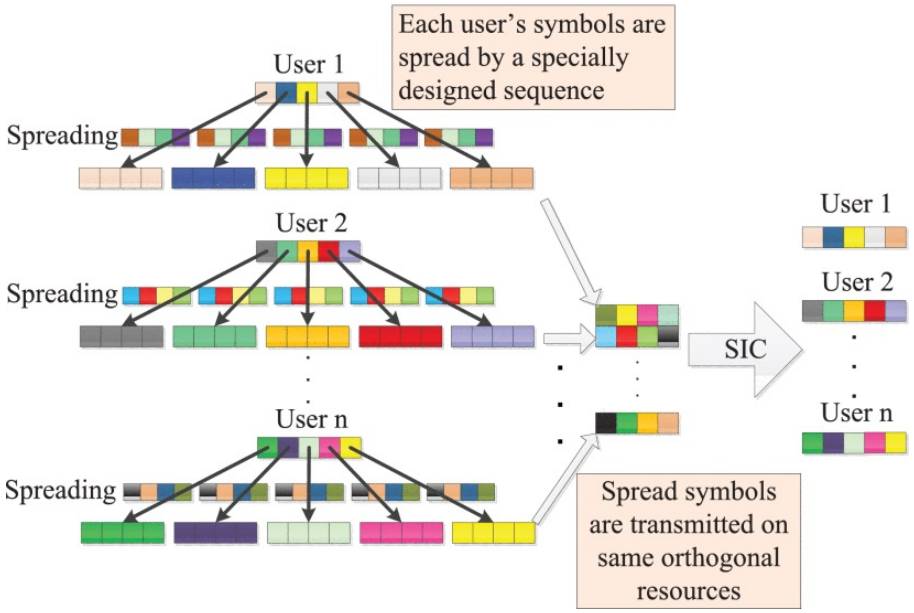

Figure 1.12: MUSA code generation and receiver structure [4]

In CDMA, user overloading is supported with SIC using long pseudo-random spreading sequences to distinguish different users. However, long codes increase the processing complexity and delay at the receiver, which, in turn, result in high power consumption with wide time/frequency delay. Therefore, in MUSA, spreading codes of short length is preferred to achieve good user overloading. For this, a very good option is the family of complex spreading code, the length of which could be short, due to the design freedom with real part and imaginary part. Such codes can be generated naturally via M-ary binary sequence with element 1,0, and -1 for both real and imaginary parts with relatively low cross correlation. In this case $M = 3$, so each element of the complex spreading code is from the set $\{0, 1, 1+i, i, -1+i, -1, -1-i, -i, 1-i\}$

where 9^{N_c} codes can be generated with code length N_c.

1.4 Preliminaries For Iterative NOMA Detection

For the code domain NOMA solutions, there are two class of state-of-the-art receivers for MUD one of which is MPA based on the FG and SPA, the other is MMSE-SIC receiver where MMSE filtering is applied with iterative SIC. MPA based receivers are mostly adopted for the SCMA reception whereas the MMSE-SIC is used for the detection of MUSA sequences [4]. The proposed UMPA-BDF receiver architecture is also based on MPA with FG/SPA where unwhitened observations are processed at symbol time, therefore the FG/SPA structure is different than the state-of-the-art MUD based SCMA MPA. In this section, FG and SPA concept will be introduced first with a simple message passing example with given FG. Then, classical MPA based SCMA receiver will be explained. Lastly MMSE-SIC receiver will be briefly introduced, but we will cover MMSE-SIC in chapter 3.

1.4.1 Message Passing Algorithm for Reduced Complexity NOMA Detection

This approach takes advantage of graph structure specifying conditional independence relations among nodes.

1.4.1.1 Factor Graph Sum Product Algorithm

Factor graph which is a probabilistic graphical model represents the product structure of a function, and contains factor nodes and variable nodes [29]. Since graph structure specifies conditional independence relations among nodes, it simplifies the results most of the time. Marginal and conditional probabilities can be efficiently calculated by passing messages on the factor graph, this is called sum-product algorithm also named as belief propagation. The marginal probability of the node n among N nodes

can be defined as:

$$p(x_n) = \sum_{x_1} \cdots \sum_{x_n-1} \sum_{x_n+1} \cdots \sum_{x_N} p(x_{1:N}) \tag{1.1}$$

where $p(x_{1:N})$ is the joint probability function which can be written as a product of factors $f_s(x_s)$ as x_s is the set of nodes.

$$p(x_{1:N}) = \prod_s f_s(x_s) \tag{1.2}$$

A message is a vector of length J, where J is the number of possible states a node can take. It is an un-normalized 'belief'. There are two types of messages which are a message μ from factor node f to variable node x $\mu_{f\to x}$, and the reverse $\mu_{x\to f}$ where u is vector of length J, and $x = 1, \ldots, K$

Messages from factors sum out all variables except the receiving one. In particular, consider a factor s f_s that connects to particular variable x_1. Denote the other variables involved in f_s by $x_{2:M}$. Then $\mu_{f\to x_1}(x)$ becomes,

$$\mu_{f_s\to x_1}(x_1) = \sum_{x_2} \sum_{x_3} \cdots \sum_{x_M} f(x_1, x_2, \ldots, x_M) \prod_{i\neq 1}^{M} \mu_{x_i\to f_s}(x_i) \tag{1.3}$$

Messages from variables are the product of all incoming messages except the message from the receiving factor

$$\mu_{x_i\to f_s}(x_i) = \prod_{f_j\in F_x - \{f_s\}} \mu_{f_j\to x_i}(x_i) \tag{1.4}$$

where $f_j \in F_x - \{f_s\}$ is the set of vectors connected to x_i, excluding f_s. In MPA, marginals are product of all incoming messages from neighbor factors.

$$p(x) \propto \prod_{f\in F_x} \mu_{f\to x}(x) \tag{1.5}$$

Consider the example FG below in Figure 1.13, and let us try to find marginal probability $p(w)$

$$p(w) = \sum_v \sum_x \sum_y \sum_z f_1(v, w) f_2(w, x) f_3(x, y) f_4(x, z) \tag{1.6}$$

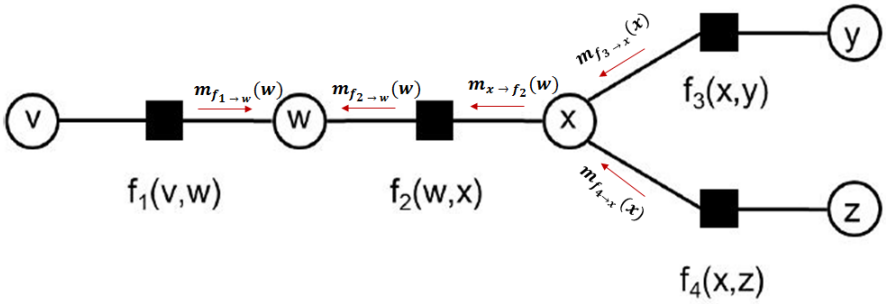

Figure 1.13: Example FG Structure [6]

$$p(w) = \underbrace{\left[\sum_{v} f_1(v,w)\right]}_{m_{f_1\to w}(w)} \underbrace{\left[\sum_{x} f_2(w,x) \left[\underbrace{\left[\sum_{y} f_3(x,y)\right]}_{m_{f_3\to x}(x)} \underbrace{\left[\sum_{z} f_4(x,z)\right]}_{m_{f_4\to x}(x)}\right]\right]}_{m_{f_2\to w}(w)} \tag{1.7}$$

Writing $p(w)$ in 1.6 brings $\mathcal{O}(K^5)$ complexity during the implementation. In Equation 1.7, sums of products becomes products of sums of all messages from neighboring factors to variables, as a result, with a naive implementation the complexity can be reduced to $\mathcal{O}(K^2)$ [6].

1.4.1.2 Max Log MAP Detection (Jacobian Algorithm)

The complexity of MAP algorithm can be significantly reduced via Max Lop MAP algorithm [30], avoiding complex multiplication process and reducing the number of summation. We use max-log MAP algorithm to simplify the messages in FG in UMPA-BDF in [31] for a smooth implementation. Max-Log algorithm can simply be defined as

$$\max^*(x_1, x_2, \ldots, x_n) = \ln\left(\sum_{i=1}^{n} e^{x_i}\right) \tag{1.8}$$

In Max-Log MAP Equation 1.9 turns into the following:

$$p(x) = \sum_{f\in F_x} \max\left(\ln(\mu_{f\to x}(x))\right) \tag{1.9}$$

where F_x is the set of factors connected to variable node x.

1.4.2 Message Passing Algorithm for SCMA Detection

SCMA receiver is based on MPA at chip rate so that number of collisons between users are limited while decoding. Each chip is called resource element (RE). Since ISI equalization is costly in terms of the computational complexity, SCMA uses the OFDM transmission, the received signal at the RE i is given as :

$$\mathbf{y}[n] = \sum_{j=1}^{K} h_j[n]x_j + \mathbf{w}[n] \tag{1.10}$$

where n is the chip time index, $x_j = (x_{1j}, \ldots, x_{N_c j})^T$ is the SCMA codeword of user j, $h_j = (h_{1j}, \ldots, h_{N_c k})^T$ is the channel gain of $j^t h$ user and $j = 1, \ldots, K$, assuming the codeword length is N_c and $\mathbf{w}[n]$ is WGN. The set of collided users depends on the mapping matrix (V_j) by the index of the non-zero elements of the binary indicator vector $diag(\mathbf{V}_j \mathbf{V}_j^T)$. The total number of users contributing to RE is

$$d_f = (d_{f_1}, \ldots, d_{f_{N_c}})^T = \sum_{j=1}^{K} f_j. \tag{1.11}$$

The SCMA code structure is defined with FG matrix with example F where N_c = 4 and K = 6.

$$F = \begin{bmatrix} 1 & 0 & 1 & 0 & 1 & 0 \\ 0 & 1 & 1 & 0 & 0 & 1 \\ 1 & 0 & 0 & 1 & 0 & 1 \\ 0 & 1 & 0 & 1 & 1 & 0 \end{bmatrix} \tag{1.12}$$

where user node j-column and RE node i-row are connected if and only if $(F)_{ij}$=1. According to the given example F matrix the corresponding FG structure given in Figure 1.14

As a result, the set of user nodes connected to RE i is defined as $L_n = j|(\mathbf{F}_{ij} = 1, \forall j,$ and the received signal is rewritten as

$$\mathbf{y}[n] = \sum_{j \in L_n} h_j[n]x_j + \mathbf{w}[n] \tag{1.13}$$

Receiving the $\mathbf{y}[n]$ MUD based on MPA can be performed for the SCMA symbol detection. In FG based iterative MUD, messages can be passed between variable and

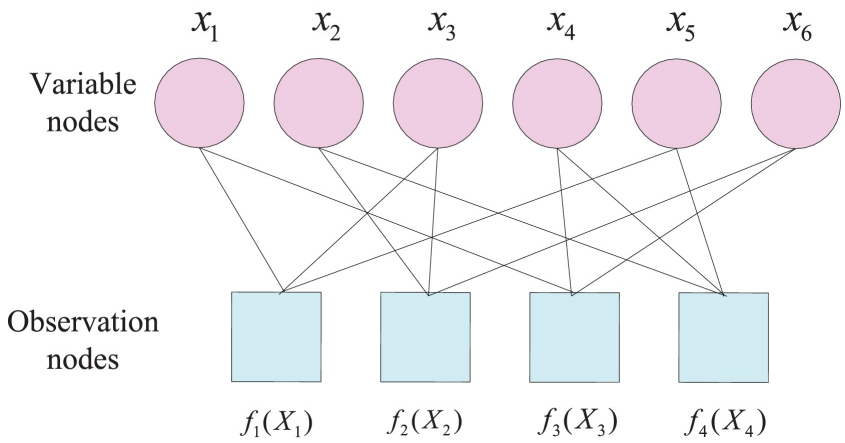

Figure 1.14: FG representation of SCMA with $K = 6, N_c = 4, d = 2$ [4]

factor nodes. A message represents the reliability of the variable associated to each edge with a soft value. Marginal distributions can be accurately calculated by limited number of iterations [4] In SCMA, given alphabet $\mathcal{X}$ optimum MAP detection of $\mathbf{x}$ where $\mathbf{x} = [x_1, x_2, ..., x_K]^T$ is given as

$$\hat{x}_k = \arg\max_{a \in \mathcal{X}} \sum_{\substack{\sim\{x_k\} \\ x_k = a}} p(\mathbf{x}|\mathbf{y}) \tag{1.14}$$

where $\sim \{x_k\}$ means all variables except x_k. Assuming uniformly distributed transmitted symbols and noise are identically and independently distributed, Equation 1.14 can be reorganized using the Bayes' rule:

$$\hat{x}_k = \arg\max_{a \in \mathcal{X}} \sum_{\substack{\sim\{x_k\} \\ x_k = a}} \prod_{n=1}^{N_c} p(y_n|x_n), \tag{1.15}$$

where $p(y_n|x_n)$ is Gaussian distributed. The $\prod_{n=1}^{N_c} p(y_n|x_n)$ term in Equation 1.15 is similar to the form of the decomposable joint probability function of MPA. In other words this problem can be turned to marginalize product of functions to have simpler solution. Then the messages in FG can be reconfigured as in [4]. Then, at the end of an iterative message passing with T iterations the approximate marginal probability of each variable can be calculated by Equation 1.9.

1.4.3 Minimum Mean Square Error (MMSE) Successive Interference Cancellation (SIC) for NOMA Detection

MMSE-SIC receiver is an iterative receiver that adapted to maximize the output SNR while minimizing the minimum mean square error during the estimation of the transmitted signal. SIC is applied in each iteration for MUD which decodes the user with highest SNR in each iteration [7]. MMSE-SIC is the state-of-the-art design for the code domain NOMA MUSA scheme and the other NOMA schemes with spreading sequences. It is sensitive to the error propagation due to the SIC [22], and creates error floor in the BER results. Moreover, there is little work in the literature that combines the massive MIMO applications and MMSE-SIC receiver for MUSA and the other code domain NOMA schemes. We will cover this issue with the details of MIMO MMSE-SIC receiver architectures in Chapter 3 .

1.5 Outline and Contribution of the Thesis

The main contribution of the thesis can be explained as the following:

- Characterization of discrete time equivalent of general uplink MIMO NOMA MAC with linear channels impaired by additive white Gaussian Noise (AWGN) at symbol rate by utilizing the channel and code correlations of each user (Chapter 2).
- Implementation and derivation of the MIMO extension for the mathematically formed iterative low complexity Ungerboeck Type Message Passing Algorithm with Bidirectional feedback (UMPA-BDF) in [32], [31] using SCMA and MUSA codes, for multi-user scenerio with the Jacobian logaritm (Max-log MAP algorithm) in wideband dispersive gaussian channels where the modulation selection can be both singlecarrier and multicarrier. Additionally, It removes the block equalization and use of cylic prefix/suffix requirements thanks to the bidirectional feedback operation (Chapter 2).
- Implementation of the UMPA-BDF receiver combined with the state-of-the-art minimum mean square error successive interference cancellation (MMSE-SIC)

algorithm for MIMO channels with MUSA codes in single tap fading channels (Chapter 3).

- Obtaining bit error rate (BER) and achievable information rate (AIR) simulation results for the implemented receiver structure by varying the number of antennas, overloading conditions, code lengths and number of channel taps, and comparing them with the matched filter bounds.(Chapter 4).

In this thesis, we will propose effective solutions to most of the main challenges of the code domain NOMA schemes explained in [3] in 2019 which are reduced complexity receiver design, complicated high dimensional codebook design, MIMO support and loading scalability issues. Our solutions will introduce a generic low complexity MIMO compatible UMPA-BDF receiver structure and application with MUSA NOMA scheme which can employ overloading without needing a multi-constellation codebook design. In addition to using the Generalized Mutual Information (GMI) concept, AIR analysis of the proposed receiver is done for both SCMA and MUSA coding schemes under many different scenarios. Moreover, in this work, the state-of-the-art MMSE-SIC algorithm performance is surpassed by using UMPA-BDF and MMSE-SIC combination.

In this first introductory chapter, firstly, we have covered briefly the conventional MA schemes from 1G to 5G and definition of the NOMA concept with power domain and code domain NOMA types. Then, the current state-of-the-art iterative NOMA detection techniques are discussed by giving the details of the factor graphs and sum product algorithm.

In the second chapter, firstly, code domain NOMA based uplink transmission scheme is modeled in discrete time for MIMO MAC by using the channel and code mathed filtered outputs. While deriving the model, unlike Forney Model where whitening filter is used after channel matched filters, Ungerboeck type unwhitened observations are directly used at symbol rate. Then, using the derived signal model and FG/SPA frameworks in [29,33], UMPA-BDF algorithm will be explained by giving the details of bidirectional ISI and MUI mitigation and the required message scheduling for the proposed MPA. In addition, complexity analysis of the proposed receiver architecture will be analyzed in this chapter.

In the third chapter, for the non-orthogonal MUSA coding scheme, MIMO compatible MMSE SIC algorithm will be derived. Having covered the details of MMSE-SIC, combination of the MMSE-SIC and UMPA-BDF algorithm will be introduced which significantly improves the state-of-the-art MMSE-SIC BER and AIR performance.

In the fourth chapter, firstly, our performance benchmarks which are the Generalized Mutual Information (GMI) for AIR analysis and overloading concept will be explained. Then, numerical BER and AIR performance results will be presented for the different MIMO MAC scenarios for UMPA-BDF and MMSE-SIC aided UMPA-BDF utilizing the SCMA and MUSA schemes.

1.6 Notation

In this section, the mathematical notation which will be used throughout this thesis will be described. There are several variables and equations in order to create a general framework for the uplink NOMA communication system and a receiver design compatible with that framework. To increase readability of these thesis, we will introduce general rules of notation which is valid throughout the thesis for all variables and equations.

Scalar variables are noted as small italic letters like a whereas the vector variables are expressed with small and bold letters like $\mathbf{b}$ without considering whether the variable is random or deterministic. That is, no special notation is used to differentiate random and deterministic variables. The variables in matrix form are denoted as capital bold letters like $\mathbf{C}$. These notations do not change whether the variable is used as a subscript or superscript. As for the estimated variables, they are denoted with a hat sign above the true variable. For example, if a is a scalar value, its estimation is denoted as $\hat{a}$. Throughout this thesis, the auto-correlation vector of a scalar random variable a is denoted as $\mathbf{r}_a$. Similarly, auto-correlation matrix of a vector random variable $\mathbf{b}$ is denoted as $\mathbf{R}_\mathbf{b}$.

The explanations of each variable used in this thesis can be found in the section that it is first defined. However, the notation rules should make the readers understand the meaning of the variable names easily.

CHAPTER 2

GENERIC SYSTEM MODEL AND A REDUCED COMPLEXITY UNGERBOECK TYPE MAP RECEIVER ARCHITECTURE

In this chapter, firstly, code domain NOMA based uplink transmission schemes are modeled where a total of K users are assumed to be present in the MIMO MAC. The discrete time equivalent model for such scheme is developed by using the matched filtered (MF) outputs along with the NOMA codebook correlations which will be useful for deriving the reduced complexity MUD.

Secondly, we propose an efficient two dimensional Ungerboeck factorization of code domain MIMO NOMA MAC as a generalized version of previous works in [31] and [32], which exploits low complexity MPA for MUD. In this chapter, after giving the 2–D FG/SPA framework of the proposed algorithm, Ungerboeck type Message Passing Algorithm with bidirectional feedback (UMPA-BDF) realizing iterative max-log Maximum a posteriori (MAP) detection is explained over the given framework.

2.1 Signal Model

As the number of transmitted NOMA symbols (with code length N_c and cardinality M) is assumed to be T for each user, the baseband equivalent of the transmitted signal of u^{th} user can be represented as

$$x^{(u)}[n] = \sum_{k=0}^{T-1} g_{I_k^u}^{(u)}[n - kN_c] \;\text{ for } I_k^u \in \{1, \cdots, M\}, \tag{2.1}$$

where $\left\{ g_i^{(u)}[n] \right\}_{n=0}^{N_c-1}, \; i = 1, \ldots, M, \; u = 1, \ldots, K$ are the corresponding NOMA waveforms.

Considering that each user has quasi-static MIMO channels $\mathbf{h}^{(u)}[n]$ including multi-path components for different antennas. The baseband representation of the received NOMA signal can be expressed as

$$\begin{aligned}\mathbf{y}[n] &= \sum_{u=1}^{K} \mathbf{h}^{(u)}[n] * x^{(u)}[n] + \mathbf{n}[n] \\ &= \sum_{u=1}^{K} \sum_{l=0}^{L_c-1} \mathbf{h}^{(u)}[l] x^{(u)}[n-l] + \mathbf{n}[n] \\ &= \sum_{u=1}^{K} \sum_{k=0}^{T-1} \mathbf{s}_{I_k^u}^{(u)}[n - kN_c] + \mathbf{n}[n],\end{aligned} \tag{2.2}$$

where $\mathbf{s}_m^{(u)}[n] = \mathbf{h}^{(u)}[n] * g_m^{(u)}[n]$ for $m = 1, \ldots, M,\ u = 1, \ldots, K$, and $\mathbf{n}[n]$ is the AWGN vector. There are N antenna elements at the receiver side.

Having obtained the received signal expression and assuming the symbol synchronization is realized perfectly, the MF outputs sampled at symbol rate can be represented by Equation 2.3 as the $(\mathbf{s}_m^{(u)}[-n])^{\mathrm{H}}$ denotes both the channel and code MF expression from the definition of $\mathbf{s}_m^{(u)}[n]$. That MF operation in Equation 2.3 yields cross correlation components in Equation 2.4 including inter-channel and inter-code correlations of different users which is nonzero only for $-(L-1) \leq k \leq L-1$ where $\left(L = \left\lceil \frac{L_c + N_c - 1}{N_c} \right\rceil\right)$ is the effective channel length in terms of symbol period:

$$r_m^{(u)}[k] \triangleq \left(\mathbf{s}_m^{(u)}[-n]\right)^{\mathrm{H}} * \mathbf{y}[n] \Big|_{n=kNc}, \tag{2.3}$$

$$\begin{aligned}R_{m_1,m_2}^{(u_1,u_2)}[k] &= \left(\mathbf{s}_{m_1}^{(u_1)}[-n]\right)^{\mathrm{H}} * \mathbf{s}_{m_2}^{(u_2)}[n] \Big|_{n=kN_c} \\ &= \sum_{l=0}^{L_c+N_c-2} \left(\mathbf{s}_{m_1}^{(u_1)}[l]\right)^{\mathrm{H}} \mathbf{s}_{m_2}^{(u_2)}[kN_c + l].\end{aligned} \tag{2.4}$$

We call the cross correlation term in Equation 2.4 as Ungerboeck Correlation Metric (UCM), and it will be used directly in the proposed receiver architecture for MUD. In the following equations, we try to express UCM in terms of NOMA code correlations and users' channel separately.

By defining $\mathbf{H}^{(u)} \triangleq \left[\mathbf{h}^{(u)}[0]\ \ \mathbf{h}^{(u)}[1] \cdots\ \ \mathbf{h}^{(u)}[L_c - 1]\right]_{N \times L_c}$ and, UCM $R_{m_1,m_2}^{(u_1,u_2)}[k]$

given in Equation 2.4, can be re-expressed more explicitly for the MIMO MAC as

$$R_{m_1,m_2}^{(u_1,u_2)}[k] = \mathrm{Tr}\left\{\mathbf{H}^{(u_2)}\mathbf{G}_{m_1,m_2}^{(u_1,u_2)}[k]\left[\mathbf{H}^{(u_1)}\right]^{\mathrm{H}}\right\}, \tag{2.5}$$

$$\left[\mathbf{G}_{m_1,m_2}^{(u_1,u_2)}[k]\right]_{(l_1,l_2)} = r_{g,m_1,m_2}^{(u_1,u_2)}\left[kN_c - (l_1 - l_2)\right] \tag{2.6}$$

where $\mathbf{G}_{m_1,m_2}^{(u_1,u_2)}[k]$ is an $L_c \times L_c$ Toeplitz matrix exhibiting the NOMA waveform correlations at different delays so that $(l_1, l_2)^{th}$ element of the matrix is given in Equation 2.6 which is named as Code Correlation Metric (CCM). In Equation 2.6, $r_{g,m_1,m_2}^{(u_1,u_2)}[n] \triangleq \left(g_{m_1}^{(u_1)}[-n]\right)^* * g_{m_2}^{(u_2)}[n]$ showing the cross correlation between m_1^{th} signaling waveform of u_1^{th} user and m_2^{th} signaling waveform of u_2^{th} user.

2.2 Equivalent Wideband MIMO Channel based Waveform Correlations

By using UCM in Equation 2.5, the MF outputs in Equation 2.3 can be rewritten as

$$\begin{aligned} r_m^{(u)}[k] &= \sum_{v=1}^{K}\sum_{l=0}^{T-1} R_{m,I_l^v}^{(u,v)}[k-l] + \mathbf{v}_m^{(u)}[k] \\ &= \sum_{v=1}^{K}\sum_{l=-(L-1)}^{L-1} R_{m,I_{k-l}^v}^{(u,v)}[l] + \mathbf{v}_m^{(u)}[k], \end{aligned} \tag{2.7}$$

Then, the MF outputs of each user, yielding the sufficient statistics, can be fully expressed as in the following vector-matrix form:

$$\mathbf{r}^{(u)}[k] = \sum_{v=1}^{K}\sum_{l=-(L-1)}^{L-1} \mathbf{R}^{(u,v)}[l]\,\mathbf{c}^{(v)}[k-l] + \mathbf{v}^{(u)}[k], \tag{2.8}$$

$$\left[\mathbf{R}^{(u,v)}[l]\right]_{(m_1,m_2)} = R_{m_1,m_2}^{(u,v)}[l] \;\text{ for } m_1, m_2 = 1, \ldots, M-1 \tag{2.9}$$

where

- $\mathbf{r}^{(u)}[k] = \left[r_1^{(u)}[k]\,,\, r_2^{(u)}[k]\,,\, \ldots\,,\, r_M^{(u)}[k]\right]^{\mathrm{T}}$ for $u = 1\ \ldots\ , K$ in Equation 2.8.
- $\mathbf{R}^{(u,v)}[l]$ is the $M \times M$ sampled cross-correlation matrix of the signaling waveforms of u^{th} and v^{th} user passing through the MAC.

- $\mathbf{c}^{(v)}[k]$ is the $M \times 1$ column vector whose m^{th} element is 1 if the m^{th} signaling waveform of v^{th} user is transmitted at k^{th} epoch. It can be considered as the equivalent codeword index of the NOMA codebook. For example, if $M = 4$ and $I_k^v = 3$, then $\mathbf{c}_k^{(v)} = [0\ 0\ 1\ 0]^T$ [31].

- $\mathbf{v}^{(u)}[k]$ is the correlated noise vector sequence for u^{th} user with $\mathbb{E}\left\{\mathbf{v}^{(u)}[k]\left(\mathbf{v}^{(u)}[k-l]\right)^{\mathrm{H}}\right\} = \left[\mathbf{R}^{(u,v)}(l)\right] N_0$.

The model in Equation 2.8 characterize a general uplink MIMO NOMA channel impaired by AWGN at symbol rate based on UCMs [31].

2.3 Ungerboeck Type Channel Factorization for Belief Propagation

In this receiver design, Ungerboeck type observation model at symbol rate is adopted, which removes the excessive computation needs caused by chip-rate processing for the channels with large delay spreads. Unlike conventional Forney's algorithm where noise whitening filter after channel matched filtering (CMF) is required, detection algorithm is directly applied to the unwhitened observations in the Ungerboeck model.

In this proposed FG/SPA framework, complete state reduction with decision feedback is carried out. Thus, in order to provide sufficient information to operate maximum likelihood sequence estimation (MLSE), UMPA-BDF holds a surviving path which is updated in each iterations with the help of BDF.

From the Ungerboeck ML metric in [31], the proportional joint a posteriori probability (APP) of the NOMA symbols can be factored with log-likelihood form as follows:

$$\begin{aligned}\ln\left(P\left\{\{I_k^u\}_{\forall k,u} \,\middle|\, \{\mathbf{r}^{(u)}[k]\}_{\forall k,u}\right\}\right) \propto \sum_{k=0}^{T-1}\sum_{u=1}^{K}\Big(&\phi_k^u(I_k^u) + \psi_k^u(I_k^u) \\ &+ \mathrm{P}\left(I_k^u\right)\sum_{v=1,v\leq u}^{K}\kappa_k^{u,v}(I_k^u, I_k^v)\Big)\end{aligned} \tag{2.10}$$

where

$$\phi_k^u(I_k^u) = 2\,\mathrm{Re}\left\{r_{I_k^u}^{(u)}[k]\right\} - R_{I_k^u,I_k^u}^{(u,u)}[0] \tag{2.11}$$

$$\psi_k^u(I_k^u) = -2\,\mathrm{Re}\left\{\sum_{l=1}^{L-1} R_{I_k^u,\hat{I}_{k-l}^u}^{(u,u)}[l]\right\} \tag{2.12}$$

$$\begin{aligned}\kappa_k^{u,v}(I_k^u, I_k^v) = -2\,\mathrm{Re}\Bigg\{ & R_{I_k^u,I_k^v}^{(u,v)}[0] + \sum_{l=1}^{L-1} R_{I_k^u,\hat{I}_{k-l}^v}^{(u,v)}[l] \\ & + \sum_{l=1}^{L-1} R_{I_k^v,\hat{I}_{k-l}^u}^{(v,u)}[l]\Bigg\}\end{aligned} \tag{2.13}$$

For user u and at time k, $\phi_k^u(I_k^u)$ shows the channel and code MF output of index I_k^u; $\psi_k^u(I_k^u)$ corresponds to inter-symbol interference (ISI), whereas $\kappa_k^{u,v}(I_k^u, I_k^v)$ represents multi-user interference (MUI) to u^{th} user due to v^{th} user.

The resulting 2–D FG based on the Ungerboeck MIMO MAC model in Equation 2.8 is shown in Figure 2.1. Only the connections between u^{th} and v^{th} users are demonstrated for convenience. This FG has cycles of length 6 [31]. Since cycles are present with the ISI channel, the SPA applied to this graph is iterative and leads to an approximate computation of the marginal APPs. Luckily, it is known that having cycles with length greater than 4 is sufficient to obtain good approximations to the actual APPs [34] [31].

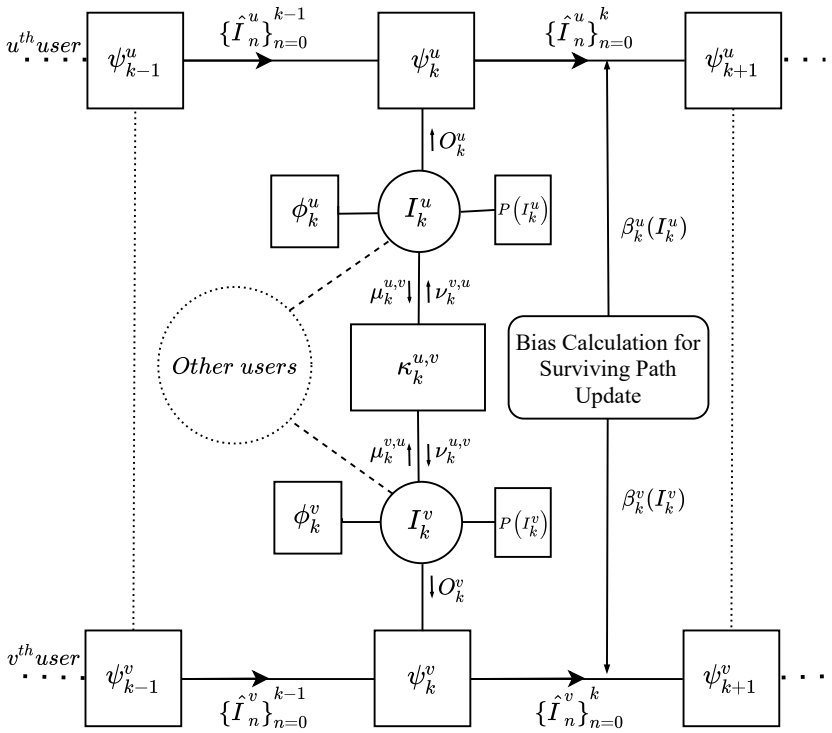

Figure 2.1: Ungerboeck Type Factor Graph for Belief Propagation

2.4 Ungerboeck Type Message Passing Algorithm with Bidirectional Decision Feedback (UMPA-BDF) for NOMA Detection

Based on given Ungerboeck type FG in Figure 2.1, by using the SPA framework in [35], UMPA-BDF has the following rules for message update while performing the max-log MAP detection:

$$O^u_k(I^u_k) = \mathrm{P}\left(I^u_k\right) + \phi^u_k(I^u_k) + \sum_{v=1, v\neq u}^{K} \nu^{v,u}_k(I^u_k) \tag{2.14}$$

$$\nu^{v,u}_k(I^u_k) = \max_{I^v_k}\left(\mu^{v,u}_k(I^v_k) + \kappa^{u,v}_k(I^u_k, I^v_k)\right) \tag{2.15}$$

$$\mu^{u,v}_k(I^u_k) = \psi^u_k(I^u_k) + O^u_k(I^u_k) - \nu^{v,u}_k(I^u_k) \tag{2.16}$$

$$\hat{I}_k^u = \arg\,\max_{I_k^u} \left(\psi_k^u(I_k^u) + O_k^u(I_k^u) - \beta_k^u(I_k^u)\right) \tag{2.17}$$

In Figure 2.1, $\nu_k^{v,u}(I_k^u)$ performs the MUI interference cancellation that tries to eliminate the most likely symbol of v^{th} user, interfering to u^{th} user's signal during the BDF operation. While calculating MUI, the probabilities $\mu_k^{v,u}(I_k^v)$ in Equation 2.15 representing the likelihood of v^{th} user interference on user u if the user v sent I_k^v. In Equation 2.14, $O_k^u(I_k^u)$ carries the MF outputs of u^{th} user where the estimated MUI terms due to multiple users are subtracted.

2.4.1 Bias Term and Bidirectional Feedback Approach

It is known that Ungerboeck type receiver with decision feedback suffers from correct path loss even in the noiseless regime [32], [36]. This phenomenon is caused by the untreated anti-causal interference. The precursor ISI left after CMF and code MF operation in Equation 2.8 is the source of this anti-causal interference. The bias term $\beta_k^u(I_k^u)$ in Equation 2.18 of user u is calculated by hard tentative decisions about future symbols, and compensated in the forward surviving path construction in Equation 2.17, together with the causal ISI term carried by $\psi_k^u(I_k^u)$ during the BDF operation.

$$\beta_k^u(I_k^u) = 2\,\mathrm{Re}\left\{\sum_{v=1}^{K}\sum_{l=1}^{L-1} R^{(v,u)}_{\hat{I}_{k+l}^v, I_k^u}[l]\right\} \tag{2.18}$$

$$\ln\left(P\left\{I_k^u \middle| \{\mathbf{r}^{(v)}[l]\}_{\forall l,v}\right\}\right) \propto \psi_k^u(I_k^u) + O_k^u(I_k^u) - \beta_k^u(I_k^u) \tag{2.19}$$

Finally, the log-marginal NOMA symbol APPs of u^{th} user is proportional to the expression in Equation 2.19, and the argument that maximizes Equation 2.19) for k^{th} NOMA codeword gives the corresponding MAP symbol detection. Since there is only one state in the receiver design, the APP calculation in Equation 2.19 and tentative decision expression in Equation 2.17 are the same.

2.4.2 Message Scheduling

Algorithm 2.1 UMPA-BDF

Input: MF Output $\mathbf{r}^{(u)}[k]$ in Equation 2.8 and Ungerboeck Correlation Metric (UCM) $R_{m_1,m_2}^{(u_1,u_2)}[k]$ in Equation 2.5

Output: NOMA symbol sequences $\left\{\hat{I}_k^u\right\}$ in Equation 2.17

Initialization: Messages $\nu_k^{v,u}(I_k^u)$, $\mu_k^{u,v}(I_k^u)$ in (2.15) and (2.16) should be initialized to zero.

(While calculating metric values for $k<0$, use preamble.)

(Use the current surviving path $\{I_n^u\}_{n=0}^{k-1}$, finding the metric values.)

for $iter = 1:1:max\_iter\_number$ **do**

Forward *time domain belief* updates:

for $k=0:1:T-1$ **do**

Calculate $\phi_k^u(I_k^u)$, $\psi_k^u(I_k^u)$ and $\kappa_k^{u,v}(I_k^u, I_k^v)$ in Equation 2.11, Equation 2.12, Equation 2.13

Forward-Backward *user domain belief* updates:

for user index $u=1:1:K$ **do**

for user index $v=1:1:K$ **do**

Update the messages $\{\nu_k^{v,u}(I_k^u)\}_{u>v}$ in Equation 2.15;

end for

Update the term $O_k^u(I_k^u)$ in Equation 2.14)-;

for user index $v=1:1:K$ **do**

Update the messages $\{\mu_k^u(I_k^u)\}_{u<v}$ in Equation 2.16.

end for

for user index $v=K:-1:1$ **do**

Update the messages $\{\nu_k^{v,u}(I_k^u)\}_{u<v}$ in Equation 2.15;

end for

Update the term $O_k^u(I_k^u)$ in Equation 2.14;

for user index $v=K:-1:1$ **do**

Update the messages $\{\mu_k^u(I_k^u)\}_{u>v}$ in Equation 2.16.

end for

end for

if $iter > 1$ **then**

(Use the surviving path $\{I_n^u\}_{n=k+1}^{k+L}$ obtained from the previous iteration.)

Calculate bias $\beta_k^u(I_k^u)$ in Equation 2.18.

end if

Update survivors $\left\{\hat{I}_k^u\right\}$ in Equation 2.17 for each user.

end for

end for

Calculate APP $P\left\{I_k^u \middle| \{\mathbf{r}^{(v)}[l]\}_{\forall l,v}\right\}$ in Equation 2.19

A serial schedule, similar to the one in [34] is utilized to update the messages while using SPA in UMPA-BDF. Corresponding message scheduling for MPA of the 2–D FG in Figure 2.1 is given completely in Algorithm 26. It takes two inputs, one of them is that the CMF and code MF outputs of multiple users which comes from multiple receiver antennas. The other input is UCM in Equation 2.5 that shows the channel and user correlations. Messages in FG must be initialized first. UMPA-BDF has mainly one forward time iterations from first NOMA symbol to last one. In each time, forward and backward two user domain process is required in order to reduce the effect of MUI in the MF outputs. At the end of the user iterations, a tentative decisions of NOMA symbols for each user is made considering the ISI and bias effects on the MF outputs. Usually 6 iterations of these are required to calculate approximately accurate APPs for the NOMA symbols of each user in the MAC.

The entire UMPA-BDF receiver architecture for an uplink NOMA for MIMO channels is summarized in Figure 2.2. It is operated on unwhitened observations without need of any computationally expensive operations like pre-filtering (requiring matrix inversions) since these operations are problematic especially for channels with long memory and time varying environments where the use of adaptive algorithms or short packet is indispensable [32]. One of the main advantages of UMPA-BDF stems from the Ungerboeck factorization exploiting ChDMA, and separates users both in code and channel domain with the help of multiple antennas. Thus, equalization on dispersive fading channels with long memory can be applied efficiently with the proposed receiver.

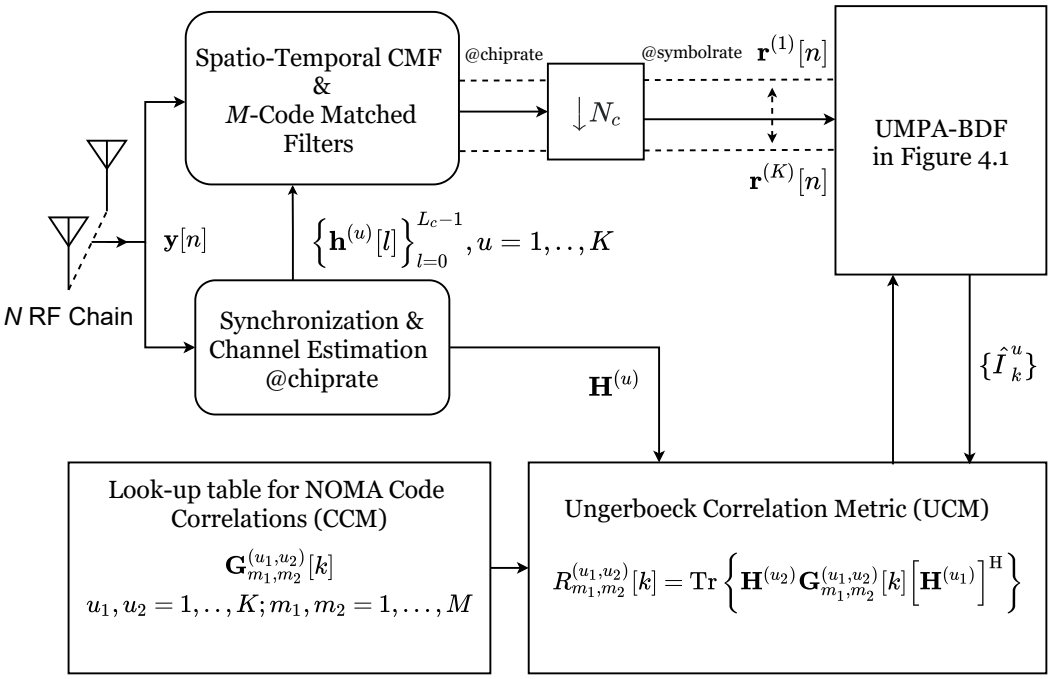

Figure 2.2: A Complete Ungerboeck Type Receiver Architecture for Code Domain NOMA Uplink Transmission

2.4.3 Computational Complexity Comparison

In terms of computational complexity, UMPA-BDF requires two nested user domain loop in order to update the messages for belief propagation. Also, it makes two separate M sized comparison in Equation 2.15 and Equation 2.17 while calculating the estimated MUI and making tentative decisions. Each of these computations are done in all iterations. Since number of iterations and M sized comparisons have a linear effect on computational complexity as $2\mathcal{O}(M)$ and $\mathcal{O}(numberofiteration)$, the determinant factor deciding the complexity of UMPA-BDF is number of user in MAC. Therefore the computational complexity of UMPA-BDF is proportional with $O(K^2)$ as the dominant factor is number of user. Moreover, UMPA-BDF algorithm utilizes logarithmic-domain MPA where the computational complexity degrades more than $\%50$ as compared to classical MPA structures with only negligible performance loss in practical applications [4]. In MIMO scenario, number of antenna N does not change the computational complexity of UMPA-BDF because CMF sums all the RF-chain outputs. Unlike the other state-of-the-art receiver approaches, the complexity

of UMPA-BDF algorithm is independent from the number of interfering multipath components which dramatically increases the computational complexity.

Investigating the state-of-the-art full MPA receiver for decoding SCMA, chip rate processing is used which increases the complexity more unlike the UMPA-BDF which is implemented in symbol time. Considering the computational complexity, number of iteration is one of the linear complexity factor due to the iterative structure. However, the dominant computational load for the MPA is because of the constellation size M. Let w is the maximum number of non-zero signals superimposed on each chip or sub carrier, computational complexity of MPA is approximately $\mathcal{O}(M^w)$ which is lower than the ML receiver complexity $\mathcal{O}(M^K)$. However in a massive connectivity scenario as the number of users K increases, w must increase.Therefore, computational complexity of the MPA receiver has exponential growth with K [4]. For example, in a typical scenario $w = 3$ for $N_c = 4$ and $K = 6$ under $\%150$ loading, the complexity of MPA is $\mathcal{O}(M^3)$.

As for the state-of-the-art MMSE-SIC receiver which is actively used for MUSA coding scheme, due to the iterations, matrix inversion and the maximum SNR searching process with size K in SIC; the computational complexity is approximately $\mathcal{O}(K^3)$ where the number of user is dominant factor [4]. Different than the MPA, the MMSE-SIC complexity is not exponentially depends on M. As a result, it looks more suitable for a typical massive MIMO scenarios.

In the Table 2.1 approximate computational complexity of ML, MPA, MMSE-SIC, and UMPA-BDF algorithms are shown.

In terms of signaling cost, UMPA-BDF only requires a training sequence in the first symbol or frame with length L the effective channel length. However, SCMA and MUSA are considered with the OFDM which requires CP overhead for the all symbols. All of the algorithms are required to use pilot signals for the channel estimation. As a future work a channel estimation algorithm can be implemented to the UMPA-BDF removing the pilot signal and channel state information requirement for the receiver. Still, for code domain NOMA schemes, receivers have to know the which codebook is used by each user where extra signaling is needed.

Table 2.1: Receiver Schemes and Complexity Comparison

Schemes	**Proposed Receivers**	**Receiver Complexity**
Generic	ML	$\mathcal{O}(M^K)$
SCMA	MPA	$\mathcal{O}(M^w)$
MUSA	SIC-MMSE	$\mathcal{O}(K^3)$
Generic (Code Domain)	UMPA-BDF	$\mathcal{O}(K^2)$

CHAPTER 3

MMSE-SIC AIDED UMPA-BDF FOR MIMO CHANNELS

In this chapter, we will particularly focus on derivation and application of the linear MMSE-SIC receiver for the MUSA codes in MIMO MAC. Optimum linear MMSE filter is derived first, then the application of the SIC algorithm will be defined. Lastly, the combination of the UMPA-BDF and MMSE-SIC algorithms will be discussed for improved NOMA detection in a MIMO MAC.

3.1 MMSE-SIC Receiver Architecture for Code Domain NOMA Schemes in MIMO Channels Compatible to Multi-Carrier Adaptations

Decorrelator bank and matched filtering are two known receiver architectures for multi-user detection [37]. However at low SNR values the performance of the decorrelator type receiver is failed due to the background Gaussian noise while matched filtering is not successful at high SNR because of the high inter-user interference. Therefore, it is required to design an optimum linear receiver that behaves like a matched filter at low SNR cases and decorrelator for a higher SNR cases, maximizing the output signal-to-interference-plus noise ratio (SINR) for all SNRs. The linear MMSE receiver makes this trade-off trying to reduce the interference whereas capturing the signal energy as much as possible, and achieves the capacity for both high and low SNR cases. Derivation of the MMSE receiver is based on a strategy that turns the colored interference noise into white additive noise by applying invertible linear transformation to the received signal.

Successive cancellation is decoding data streams sequentially,that is, decoding the signal with highest SINR values then removing it from the received signal. While

selecting and decoding the user's signal with maximum SNIR, linear MMSE receiver is utilized. This combination is called as MMSE-SIC receiver, which is an iterative receiver designed to maximize output SNR whereas minimizing the MMSE in order to achieve capacity. SIC is applied in all iterations for MUD removing the signal with highest SNR which can be considered a powerful interference for the other users. Moreover, it is shown that the MMSE-SIC receiver achieves the capacity of the fading MIMO channel [37], which makes it a good candidate for our multi-carrier NOMA decoding MAC scenarios as MSE-SIC is the state-of-the-art receiver for the MUSA schemes. One important drawback of this MMSE-SIC receiver is error propagation problem due to SIC operation, which saturates the BER curves. Although MMSE-SIC is used for MUSA detection, there is no such work in the literature that decodes the MUSA schemes in MIMO MAC.

In order to derive the MMSE filter, let y_n be the received signal of multiple users from multiple antennas, after the CMF stage in the following equation the signal becomes $z^{(u)}[n]$ which is for the u^{th} user where $\mathbf{h}_n^u$ is the MIMO channel for the user u.

$$\begin{aligned} z^{(u)}[n] &= \left(\mathbf{h}^{(u)}[-n]\right)^{\mathrm{H}} * \mathbf{y}[n] + \mathbf{v}^{(u)}[n] \\ &= \sum_{v=1}^{K} \sum_{l=-(L_c-1)}^{L_c-1} r_h^{(u,v)}[l] x^{(v)}[n-l] + \mathbf{v}^{(u)}[n] \end{aligned} \tag{3.1}$$

In Equation 3.1, $r_h^{(u,v)}[l] = \left(\mathbf{h}^{(u)}[-l]\right)^{\mathrm{H}} * \mathbf{h}^{(v)}[l]$ for $u = 1, \ldots, K$ and $\mathbf{v}^{(u)}[n]$ is the colored noise after CMF. For the MIMO case, the CMF outputs of each antenna (RF chain) are summed.

Assuming perfect ISI cancellation assumption or considering $L_c = 1$ as in the case in multi-carrier transmission, the summed CMF output becomes:

$$z^{(u)}[n] = \sum_{v=1}^{K} r_h^{(u,v)}[0] x^{u}[n] + \mathbf{v}^{(u)}[n] \tag{3.2}$$

In Equation 3.2 after CMF outputs for $L_c = 1$ or perfect cancellation circumstance are shown. That is, receiver only have to deal with with MUI. In multi-carrier version of this equation, codes are carried in subcarriers which result in for k subcarriers there are $N \times 1$ observations. And, h_k definition arises showing the equivalent MIMO channel in k^{th} sub-carrier. In this section, we will continue the MMSE filter derivation

over perfect ISI cancellation case, however OFDM conversion of the equations are possible.

Let $q^{(u)}[k]$ be the $N_c \times 1$ MMSE filter input at time $k = 0, \ldots T-1$ for each user $u = 1 \ldots K$.

$$\mathbf{q}^{(u)}[k] \triangleq \left[q^{(u)}[kN_c]\ q^{(u)}[kN_c+1]\ \ldots\ q^{(u)}[kN_c+N_c-1]\right]^{\mathrm{T}} \tag{3.3}$$

NOMA code vector for the MUSA scheme can be defined as $\mathbf{g}_k^{(u)} = \mathbf{c}_{N_c\times 1}^{(u)} a_k^{(u)}$ where $a_k^{(u)}$ M-QAM symbol and $\mathbf{c}_{N_c\times 1}^{(u)}$ is the MUSA codeword that consist of randomly selected complex elements from the set $\{0, 1, 1+i, i, i-1, -1, -1-i, -i, 1-i\}$ that we selected. After putting the MUSA codeword definition into Equation 3.2, we have:

$$\mathbf{q}^{(u)}[k] = \sum_{v=1}^{K} r_h^{(u,v)}[0]\mathbf{c}^v a_k^{(v)} + \mathbf{v}^{(u)}[n] \tag{3.4}$$

where $u = 1, \ldots K$. Concatenating the $\mathbf{q}^{(u)}[k]$ for each user in a one $N_cK \times 1$ vector, we get the following equations:

$$\begin{aligned} \mathbf{r}_{mmse}[k] &= \left[\left(\mathbf{q}^{(1)}[k]\right)^{\mathrm{T}}\ \left(\mathbf{q}^{(2)}[k]\right)^{\mathrm{T}}\ \ldots\ \left(\mathbf{q}^{(K)}[k]\right)^{\mathrm{T}}\right]_{N_cK\times 1} \\ &= \sum_{v=1}^{K} \mathbf{g}^{(v)} a_k^{(v)} + \mathbf{z} \end{aligned} \tag{3.5}$$

$$\mathbf{g}_{mmse}^{(v)} = \begin{bmatrix} r_h^{(1,v)}[0]\mathbf{c}^{(v)} \\ r_h^{(2,v)}[0]\mathbf{c}^{(v)} \\ \vdots \\ r_h^{(K,v)}[0]\mathbf{c}^{(v)} \end{bmatrix}_{N_cK\times 1} \qquad v = 1, 2, \ldots, K \tag{3.6}$$

where $\mathbf{g}_{mmse}^{(v)}$ holds the inter-user channel correlation and MUSA code relation of user v. Concatenating side by side $\mathbf{g}_{mms}^{(v)}$, we define the following matrix that holds all code and channel relations for all users:

$$\mathbf{G}_{mmse} \triangleq \left[\mathbf{g}_{mmse}^{(1)}\ \mathbf{g}_{mmse}^{(2)}\ \cdots\ \mathbf{g}_{mmse}^{(K)}\right]_{N_cK\times K} \tag{3.7}$$

Apart from these, linear MMSE filter coefficients for all user can also be defined as the matrix form:

$$\mathbf{W} \triangleq \left[\mathbf{w}^{(1)}\ \mathbf{w}^{(2)}\ \ldots\ \mathbf{w}^{(K)}\right]_{N_cK\times K} \tag{3.8}$$

where $\mathbf{w}^{(v)}$ is the MMSE filter coefficients of v^{th} user.

Having seen matrix definition, MMSE receiver can be defined with the following expression:

$$\hat{\mathbf{a}}_k = \mathbf{W}^{\mathrm{H}}\mathbf{r}_{mmse}[k] \tag{3.9}$$

as $\hat{a}_k^{(m)}$ corresponds to the m^{th} column of $\hat{\mathbf{a}}_k$ showing the estimated symbols of m^{th} user.

Let $N_0 = 1/\text{SNR}$, the MMSE filter coefficient can be calculated as:

$$\mathbf{W} = \mathbf{G}_{mmse}\left[E_s\mathbf{G}_{mmse}^{\mathrm{H}}\mathbf{G}_{mmse} + N_0\mathbf{I}\right]^{-1}E_s \tag{3.10}$$

where E_s is the average symbol energy. In order to run SIC algorithm, the user with highest SINR must be found first. SINR calculation is done using the ration of estimated signal power over interference and noise power as shown in the following expression:

$$SINR^{(m)} = \frac{E_s\left|\mathbf{W}^{(m)^{\mathrm{H}}}\mathbf{g}_{mmse}^{(m)}\right|^2}{\left|\mathbf{W}^{(m)^{\mathrm{H}}}\mathbf{R}_{mmse}^{(m)}\mathbf{W}^{(m)}\right|^2} \tag{3.11}$$

where $m = 1, \ldots, K$ and $\mathbf{R}_{mmse} = E_s\mathbf{G}_{mmse}^{(m)}{\mathbf{G}_{mmse}^{(m)}}^{\mathrm{H}} + N_0\mathbf{I}$

Having found the SINR value for all users, the user with the highest SINR must be determined. Then, using the previously calculated MMSE filter coefficients of that user is obtained from the relevant column of W matrix to find the estimated symbols $\hat{a}_k^{(m)}$ of the user with highest SNR. Having known the $\hat{a}_k^{(m)}$ value, contribution of that user to Equation 3.4 is subtracted from the equation at the end of the first iteration. Then, using the new received signal expression, same steps are applied until all user's data is decoded. A block diagram of this MMSE-SIC algorithm is illustrated in the Figure 3.1

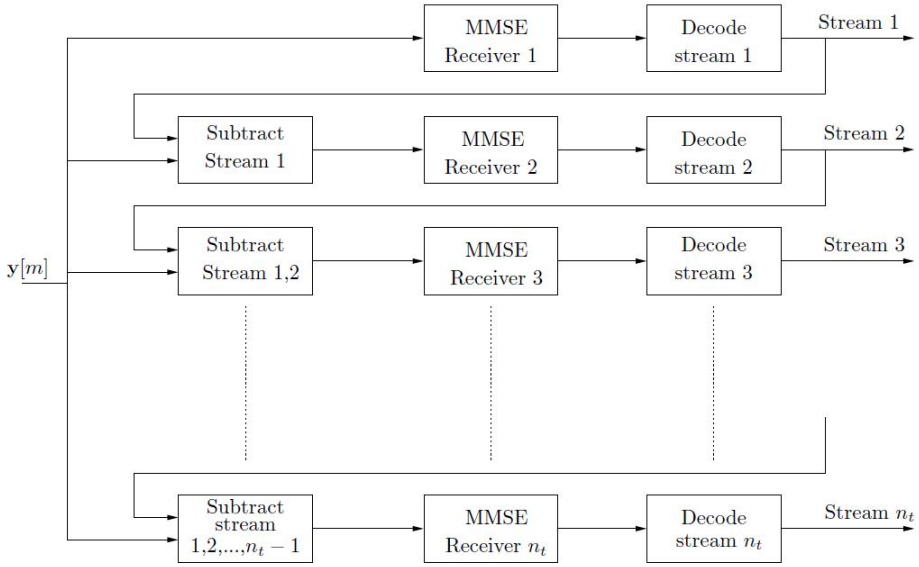

Figure 3.1: MMSE-SIC: A bank of linear MMSE receivers, and the SIC algorithm [7]

3.2 NOMA Detection with MMSE-SIC Aided UMPA-BDF

Having seen the MIMO MMSE-SIC receiver structure for decoding MUSA sequences particularly, the estimation or decoding success can be gone further using the UMPA-BDF algorithm after the MMSE-SIC to boost the performance. The corresponding results for the improvements are presented in section 4.4, and in some cases using UMPA-BDF brings up to 5-10 dB SNR gain in BER performance results. We call this combination MMSE-SIC aided UMPA-BDF receiver algorithm where instead of performing the first iteration of UMPA-BDF given in Algorithm-26 at section 2.4, MMSE-SIC receiver is carried out to have symbol estimations of all users for all k time index. Then, Algorithm-26 can continue running from iteration 2 by the symbol estimates from MMSE-SIC.

Applying MMSE-SIC instead of the first iteration of UMPA-BDF removes the need of using training sequence, reducing the signaling cost more. However, the receiver complexity is increased due to the MMSE-SIC. Particularly, the need for the knowledge of previous symbols in Equation 2.12 for $\psi_k^u(I_k^u)$ and Equation 2.13 for $\kappa_k^{u,v}(I_k^u, I_k^v)$ are not a case if the MMSE-SIC estimates are provided. Moreover, $\kappa_k^{u,v}(I_k^u, I_k^v)$ metric which holds the multi-user correlation terms is not in matrix form anymore since we

Algorithm 3.1 MMSE-SIC aided UMPA-BDF Algorithm

Input: CMF Output $z^{(u)}[n]$ in Equation 3.1, First tap of $r_h^{(u,v)}[l]$ cross correlation of user channels and Ungerboeck Correlation Metric (UCM) $R_{m_1,m_2}^{(u_1,u_2)}[k]$ in Equation 2.5

Output: NOMA symbol sequences $\left\{\hat{I}_k^u\right\}$ in Equation 2.17 and MMSE-SIC symbol estimates $\{\hat{a}_k^u\}$ in in Equation 3.9 for $u = 1, \ldots, K$

1: **for** $user - iter = 1:1:K$ **do**
2: Find MMSE weight matrix $\mathbf{W}$ with Equation 3.10 ;
3: Calculate SINR for each user with Equation 3.11 and find user with maximum SNR;
4: Find the NOMA symbol estimates $\hat{a}_k^{(m)}$ for the user with maximum SNR with Equation 3.9.
5: Update $\mathbf{y}^{(u)}[k]$ term, applying SIC.
6: **end for**
7: Using $\hat{a}_k^{(m)}$, implement Algorithm-26 at $iter = 2$ (Change $\kappa_k^{u,v}(I_k^u)$, Equation 2.12 and $\nu_k^{v,u}(I_k^u)$ metrics as required)

can trust the MMSE-SIC estimates while considering the current symbol estimates I_k^v, therefore, $\kappa_k^{u,v}(I_k^u, I_k^v)$ becomes $M \times 1$ vector where variable term is only I_k^u.

The change in structure of $\kappa_k^{u,v}(I_k^u, I_k^v)$ affects the FG message $\nu_k^{v,u}(I_k^u)$ in Equation 2.15 as:

$$\nu_k^{v,u}(I_k^u) = (\mu_k^{v,u}(I_k^v) + \kappa_k^{u,v}(I_k^u)) \tag{3.12}$$

where $\kappa_k^{u,v}(I_k^u)$ is not a function of I_k^v anymore as we use the MMSE-SIC estimations, therefore, while applying the Jacobian logarithm (Max-Log MAP) it is not required to take maximum values corresponding to I_k^v candidates.

After applying these changes, UMPA-BDF can continue running up to last iteration utilizing MMSE-SIC at first iteration, as a result, in Algorithm-26 is implemented from $iter = 2$ point with new $\kappa_k^{u,v}(I_k^u)$, Equation 2.12 and $\nu_k^{v,u}(I_k^u)$ metrics. The corresponding MMSE-SIC aided UMPA-BDF algorithm is presented in Algorithm-3.1

CHAPTER 4

BENCHMARKS AND NUMERICAL RESULTS

In this chapter, firstly our benchmarks which are the AIR and overloading will be discussed, then secondly, the numeric performance evaluation of the UMPA-BDF receiver will be studied together with SCMA and MUSA coding schemes in order to emphasize the generic structure of the proposed architecture. Particularly, we will focus on the bit error rate (BER) and AIR performances of the UMPA-BDF with a variable number of antennas under different channel and overloading conditions in the MATLAB environment using the Monte Carlo method.

4.1 Performance Analysis Based on Achievable Information Rate

Due to the complexity limitations and need for perfect channel state information which practically is not possible, mismatch decoding setups where decoding rule is sub-optimum are preferred and studied in the communication systems [38], [39]. In this section, mismatched decoding setup will be identified. For a discrete memoryless information channel (DMC) where input and output alphabets are shown as $\mathcal{X}$ and $\mathcal{Y}$, let the input sequence be $\mathbf{x} = (x_1 \dots x_n)$ and the output sequence is randomly generated from the input sequences as $\mathbf{y} = (y_1 \dots y_n)$. Given these parameters a random channel transition law can be defined as:

$$W^n(\mathbf{y}|\mathbf{x}) \triangleq \prod_{i=1}^{n} W(y_i|x_i) \tag{4.1}$$

where W is conditional probability mass function (PMF) for discrete alphabets $\mathcal{X}$ and $\mathcal{Y}$. The transmitter takes a code corresponding to symbol m among equiprobable $1, \dots, M$ points in input alphabet $\mathcal{X}$ from a codebook $C = x^{(1)}, \dots x^{(M)}$ as in the

case of NOMA schemes MUSA and SCMA. When the receiver obtains $\mathbf{y}$ vector as the channel output, it makes an estimate of the sent sequences in the decoder as the following form:

$$\hat{m} = arg \max_{j \in \{1,\ldots,M\}} q^n(\mathbf{x}^{(j)}, \mathbf{y}), \tag{4.2}$$

where $q^n(\mathbf{x}, \mathbf{y}) \triangleq \prod_{i=1}^{n} q(x_i, y_i)$ and the $q(\mathbf{x}, \mathbf{y})$ is nonnegative bounded decoding metric. When $\hat{m} \neq m$ an error occurs with average probability of error p_e in the decoding.

A rate R is achievable if for all $\sigma > 0$ there exist a code sequences C_n of length N_c with $p_e \to 0$ and $M \geq e^{N_c(R-\sigma)}$. The mismatched capacity is defined to be the maximum point of achievable rates [39]. When $q(x, y) = W(y|x)$, it corresponds to maximum-likelihood (ML) decoding which is the rule that minimizes the probability of error. In such case, mismatched capacity is the (matched) capacity as the following:

$$C = \max_{Q} I(X; Y), \tag{4.3}$$

where

$$I(X; Y) \triangleq \sum_{x,y} Q(x)W(y|x) \log \left(\frac{W(y|x)}{\sum_{\bar{x}} Q(\bar{x})W(y|\bar{x})} \right) \tag{4.4}$$

The maximum achievable information rate (AIR) is described as the mutual information (MI) in Equation 4.4, I(X;Y), of the channel. In other words, channel capacity is MI that I(X;Y) maximized over all possible input distribution $p(x)$ under average power constraint.

Considering the wireless communication, due to the numerous uncertainties in the channel, mismatched decoding is the practical case where channel $\hat{W}(y|x)$ is estimated incorrectly, however, decoder still uses this estimate as if it is correct as $q(x, y) = \hat{W}(y|x)$. Wireless communication systems are often designed to handle Gaussian noise, however most of the time non-gaussian noise is experienced in the practical systems, creating mismatched decoding environment as in the case of UMPA-BDF. Moreover, it might not possible to implement ML decoding even if the channel is known due to the complexity issues as in the case in uplink NOMA schemes presented in this thesis.

Having assumed that each symbol of each codeword is generated independently and codewords are created uniformly from the set of sequences, different AIRs have been derived for the mentioned mismatched decoding setup. One of the known AIR definitions is LM Rate (lower bound on the mismatch capacity) [40] whose proof relies on the input and output alphabets are finite. As for general alphabets, AIR definition is derived in [41] called generalized MI (GMI). In this thesis, GMI concept is employed in order to obtain a lower bound for AIR in a MAC where mismatch occurs since ML implementation is not possible due to the complexity concerns and the noise at the MF outputs are not AWGN anymore in MAC. As an analysis tool, GMI metric presented in [41] is adopted to obtain AIR and the expression is given as

$$C = \log_2 M - \mathop{\mathbb{E}}_{d,r} \left\{ \log_2 \frac{\sum_{d' \in A_d}^{K} \mathrm{p}(r|d')}{\mathrm{p}(r|d)} \right\} \tag{4.5}$$

where A_d is the modulated symbol alphabet, M is the modulation order and $\mathrm{p}(r|d')$ is the conditional probability density function (PDF) of decoded signal r given that symbol d is sent.

In [42], [43], [44] and references therein, mismatched decoding has been applied to various scenarios including ISI channels. Based on this approach the mismatched achievable rate becomes a lower bound to Equation 4.5 as

$$C_k^u = \left[\log_2 M - \mathop{\mathbb{E}}_{I_k^u, \mathbf{r}} \left\{ \log_2 \frac{\sum_{(I' \in A_c)} \mathrm{P}\left(I' \middle| \{\mathbf{r}^{(v)}[l]\}_{\forall l,v}\right)}{\mathrm{P}\left(I_k^u \middle| \{\mathbf{r}^{(v)}[l]\}_{\forall l,v}\right)} \right\} \right] \frac{1}{N_c} \tag{4.6}$$

where $\mathrm{P}\left(\hat{I}_k^u \middle| \{\mathbf{r}^{(v)}[l]\}_{\forall l,v}\right)$ is the approximate conditional marginal symbol APPs in Equation 2.19 showing pdf of decoded NOMA symbols with length N_c. In Equation 4.6, A_c represents the NOMA codebook, and M is the modulation order. After averaging the Equation 4.6 over all packet time and for all user, average AIR per user can be acquired.

4.2 Performance Analysis Based on Loading Issues

Devices or users are usually can be assigned with different time, frequency, code and and spatial domains that we call resources for the transmissions. Overloading occurs when the number of users or device in the system is more than the number of available resources. In order to use the resources efficiently, designers are trying to assign as many user as possible to a single resource as NOMA is created for this aim while considering the lower complexities at the receiver [22].

In traditional CDMA, overloading scenarios are realized through long pseudo-random spreading sequences which have low cross-correlation. However, although using long sequences supports higher user overloadings, it brings rapid increase to the receiver complexity as the number of user increases along with the transmission delays and higher power consumption. Considering these effect into account, in NOMA, MUSA and SCMA employs short spreading codes to implement overloading which in turns, reduce the receiver complexity, delay and power consumption. However one of the important drawback of LDSMA and SCMA is the lack of flexibility in terms overloading which depends on the sparsity and the dimension of complex constellation mapping. Therefore, in this thesis, user overloading performance is investigated with MUSA codes where each modulated symbol is spread by a complex spreading code of length N_c and transmitted on L time or frequency resources. If the number of users in the system is K, user overloading ration (OR) can be defined as

$$OR = \frac{K}{N_c} \tag{4.7}$$

The same OR is valid for SCMA as well. L in equation Equation 4.7 is equal to N_c in time domain for MUSA and SCMA sequences since we do not use any outer channel coding in this thesis. L could be shared orthogonal frequency resources if OFDM is used as the modulation scheme.

In the following numeric results for the MUSA coding sequences BER vs Loading and AIR vs Loading comparisons of different scenarios will be given from 50% to 400% overloading. From the simulation results we will see that BER and capacity performance of MUSA do not significantly degrade even when the user overloading ratio gets as high as 400% while using limited RF chains with UMPA-BDF re-

ceiver. It should also be noted that, multiple receiving antennas could improve the user overloading performance separating the user in spatial domain which is equivalent to using very long spreading codes. Employing as high as 400% overloading with low complexity receivers like UMPA-BDF and very low signaling cost as MUSA requires have a great potential to meet the massive connectivity requirements of 5G and beyond.

4.3 Scenarios

For the simulations, typical SCMA scheme 4 resource elements with 6 user in [20] is adopted for 4and 16 point multidimensional constellations with M-LDS and TMQAM shapes, respectively [45]. Since SCMA is not a flexible coding scheme with N_c and different overloading rates as it requires specially designed multi-constellation structures with an appropriate sparsity arrangement between codebooks of different users, we can only present scenarios under 150% loading for the SCMA scheme.

Contrary to the non-flexible format of the SCMA, as an alternative coding scheme MUSA can employ overloading without needing a particular arrangement by using low-correlation spreading sequences for different N_cs. In this work, MQAM modulated data coming from each user is spread with a MUSA codeword from a 3-ary complex set including 1, 0 and -1 with N_c.

For the performance evaluation of the proposed iterative MUD based UMPA-BDF, we use randomly selected SCMA and MUSA waveforms without any outer channel coding in a MIMO MAC where the channel taps with length L_c are Gaussian distributed and independent of each other.

Simulation parameters for different simulations are described in Table 4.1. These parameters including their notations in tabular form are used throughout the thesis.

In terms of L_c, we have two separate simulation environments. One environment is the wideband MIMO channels with Gaussian distributed channel tabs $L_c = 32$ where the ISI causing the multipath fading must be eliminated or equalized through UMPA-BDF. These types of channels are compatible to single-carrier modulation types. The

Table 4.1: Parameters used in the simulations

Name	Notation	Value
Number of NOMA symbols	—	100
Number of Iterations in UMPA-BDF	—	6
Number of users in MAC	K	2 to 64
Code length	N_c	4,8,12,16
Cardinality	M	4 or 16
Number of Antennas	N	1 to 10
Number of channel taps	L_c	1 to 32
Signal to noise ratio	E_b/N_0	0 to 30 dB

other environment is the one that is consistent with multicarrier modulation types where channel tabs are Gaussian with $L_c = 1$. In this environment, although UMPA-BDF can be directly applied, we employ the MMSE-SIC aided UMPA-BDF receiver structure where the BER and AIR performance is superior to the MMSE-SIC alone. Apart from those, we will also provide UMPA-BDF's AIR performance with higher order constellations utilizing the MUSA coding scheme with $L_c = 8$.

With these MIMO NOMA channels, we investigate the BER and AIR performance with SNR and different overloading conditions by varying the number of antennas at the receiver using SCMA and MUSA schemes without any outer channel coding.

4.4 Results

In the results part, we first show the BER vs SNR curves for iteration 1 to 6 in order to show the iterative improvement due to the UMPA-BDF algorithm. Then BER/AIR vs SNR and BER/AIR vs Loading curves will be presented for a variable number of antennas. In the simulation results, to show the performance limits, two curves which are single user matched filter bound (MFB) and UMPA-BDF with perfect BDF are inserted to the plots.

Single User MFB: This curve shows the MF detection performance of the receiver as if there were only one user in the MIMO MAC and all the ISI and MUI terms were known by the receiver. To obtain this curve, in UMPA-BDF, all of the sent symbols are accepted as known. Throughout all of the simulations, we want to approach this MFB curve as much as possible.

UMPA with perfect BDF: Unlike the single user MFB, this curve only eliminates ISI without knowing the current symbol that will be detected. In this situation, this curve focuses on the MUI, showing the multi user detection performance of the UMPA-BDF under no ISI case.

4.4.1 Wideband Channels

In Figure 4.1 and Figure 4.2, the performance variation of the proposed receiver is shown with number of self-iterations ranging from 1 to 6 where $M = 4$ and $M = 16$, $L_c = 32$ and under 150% overloading for MUSA and SCMA schemes. Due to the cycles in FG, self-iterations help the MUD to enhance its performance, and commpnsate the bias more accurately due to the iterative processes. In addition, cycles in the FG brings an error floor as the error propagates through the iterations. At the high SNR region in both figures, for iteration 6 the BER curve of UMPA-BDF sticks to the perfect BDF curve where the ISI term is entirely known. In the high SNR region the BER performance of UMPA-BDF algorithm is approximately 2 dB away from the genie aided single user in this scenario. Additionally, if the number of antennas were increased by one or two for the given scenarios, the error floor level would be much more below as we will see in the future BER results where there are variable number of antennas.

In Figure 4.3 corresponding AIR vs SNR comparisons of the BER curves in Figure 4.1 with respect to self-iterations ranging from 1 to 6 are shown. Here, our aim is to present the iterative improvement in the AIR with UMPA-BDF using both SCMA and MUSA schemes emphasizing the generic structure of the algorithm. As it can be seen from the figure, receiver can reach the maximum uncoded rate at the sixth iteration in both schemes by using UMPA-BDF which eliminates the MUI and ISI. Since SCMA has 6 users while MUSA has 12 users, MUSA needs 3 antennas as SCMA

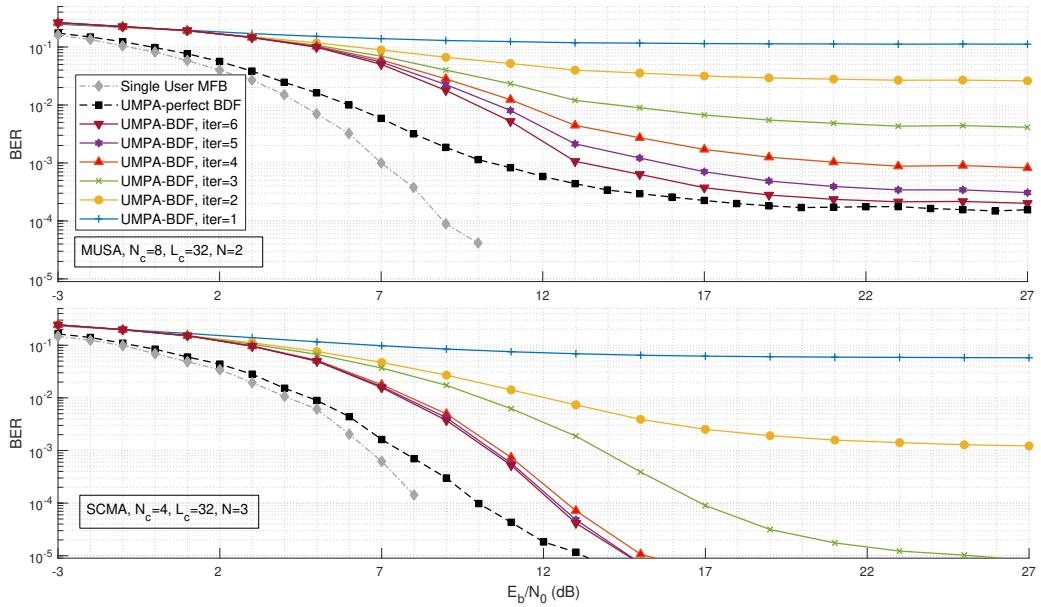

Figure 4.1: BER vs E_b/N_0 for MUSA $(N_c = 8, K = 12, N = 2)$ and SCMA $(N_c = 4, K = 6, N = 3)$ under 150% loading, $M = 4$, $L_c = 32$, Gaussian distributed tabs for MAC

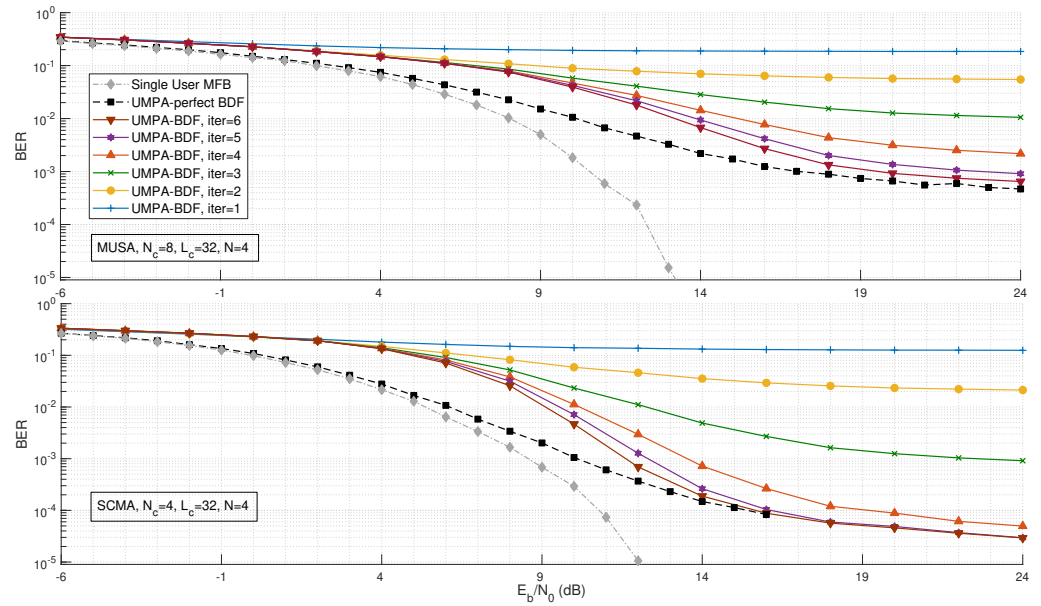

Figure 4.2: BER vs E_b/N_0 for MUSA $(N_c = 8, K = 12, N = 4)$ and SCMA $(N_c = 4, K = 6, N = 4)$ under 150% loading, $M = 16$, $L_c = 32$, Gaussian distributed tabs for MAC

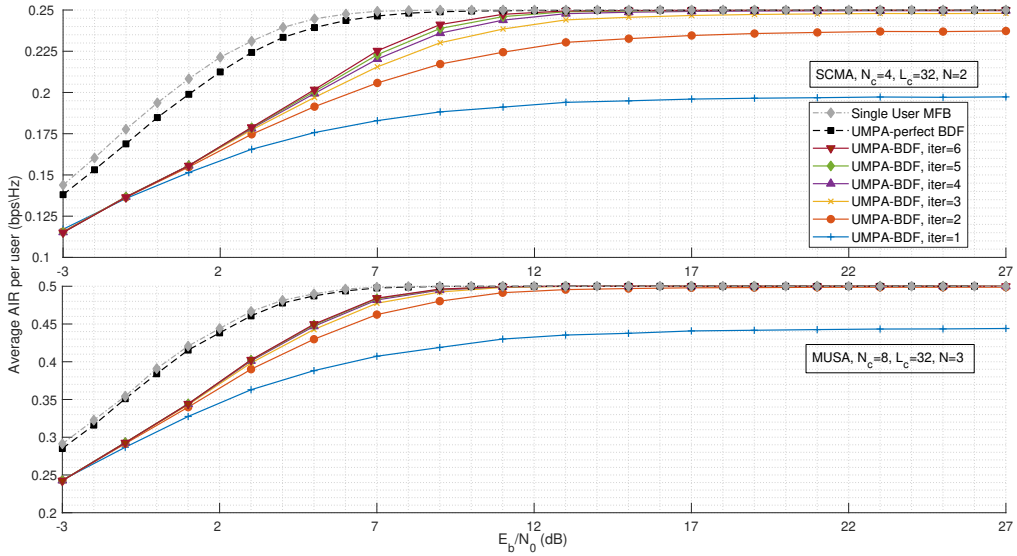

Figure 4.3: AIR vs E_b/N_0 for MUSA $(N_c = 8, K = 12, N = 2)$ and SCMA $(N_c = 4, K = 6, N = 3)$ under 150% loading, $M = 4$, $L_c = 32$, Gaussian distributed tabs for MAC

uses only 2 to mitigate the effect of MUI.

In Fig. Figure 4.4, uncoded BER performances of UMPA-BDF with respect to changing number of antenna is given for $M = 4$ for long dispersive channels. For both MUSA and SCMA schemes, BER performance dramatically enhances as the number of antenna increase which eliminates MUI more. At $N = 10$, the BER performance of single user MFB)and UMPA with perfect BDF where ISI is completely known is almost the same and the UMPA-BDF curve shows a very close achievement. The important point is, even using 2 antennas drops the BER under the 10^{-3} without using any channel coding. While investigating the BER results, it should be kept in mind that UMPA-BDF algorithm takes advantages of CMF to mitigate the effect of MUI, so it is expected that the performance is improved with longer L_cs. The same results can be verified with the corresponding AIR comparison in Figure 4.5 from the same scenario. Under 150% loading employing only two antennas (two RF chains), UMPA-BDF at the receiving ends can support the communication at maximum uncoded rate for both SCMA and MUSA schemes.

The same BER vs SNR and AIR vs SNR comparisons in Figure 4.4 and Figure 4.5 for $M = 4$ are also made for the larger constellation $M = 16$ in Figure 4.6 and Figure 4.7. This time, although $N_c = 8$ for MUSA and and 4 for SCMA, they both

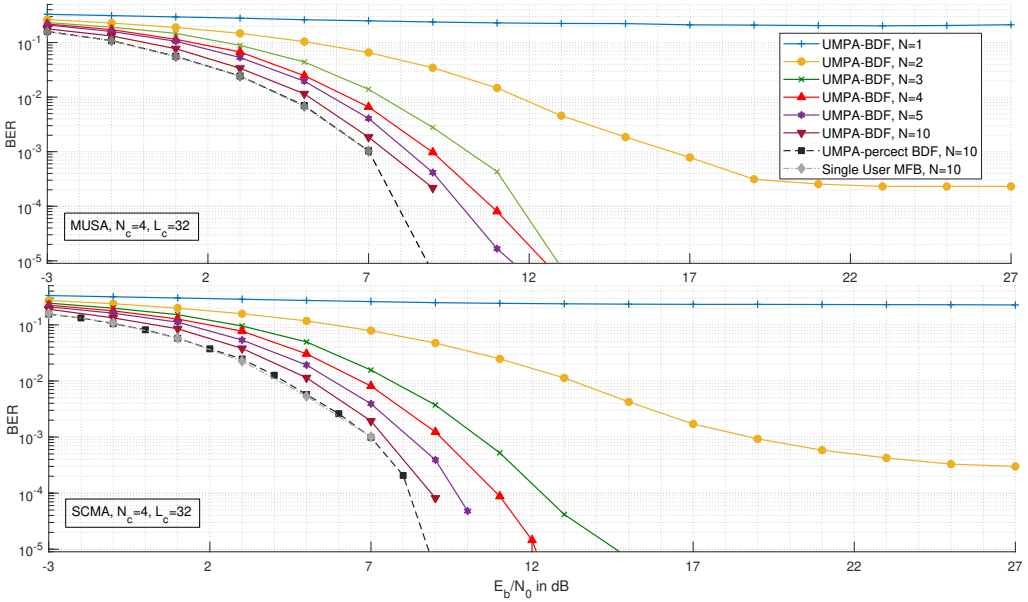

Figure 4.4: BER vs E_b/N_0 for MUSA $(N_c = 4, K = 6)$ and SCMA $(N_c = 4, K = 6)$ under 150% loading, $M = 4$, $L_c = 32$ $N = 1, 2, 3, 4, 5, 10$; Gaussian distributed tabs for MAC

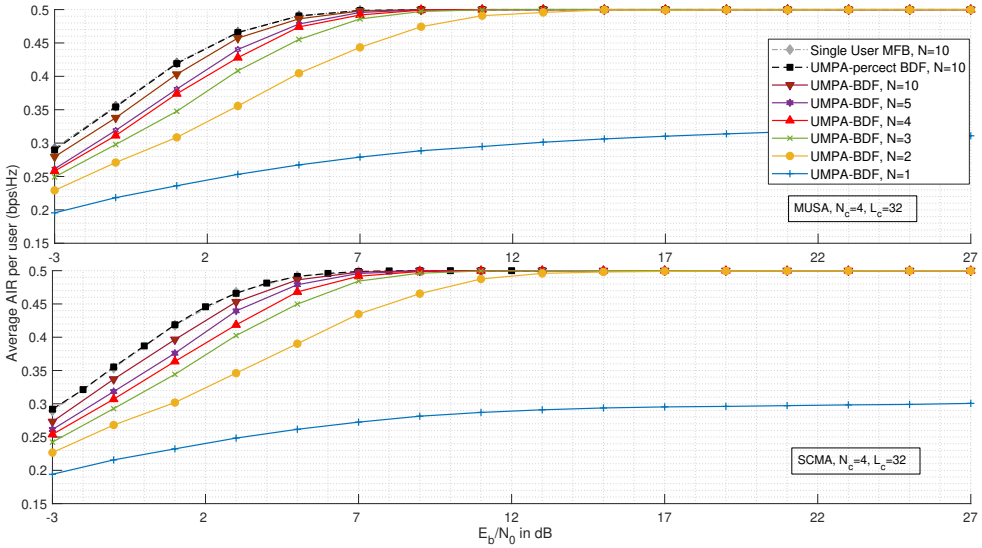

Figure 4.5: AIR vs E_b/N_0 for MUSA $(N_c = 4, K = 6)$ and SCMA $(N_c = 4, K = 6)$ under 150% loading, $M = 4$, $L_c = 32$ $N = 1, 2, 3, 4, 5, 10$; Gaussian distributed tabs for MAC

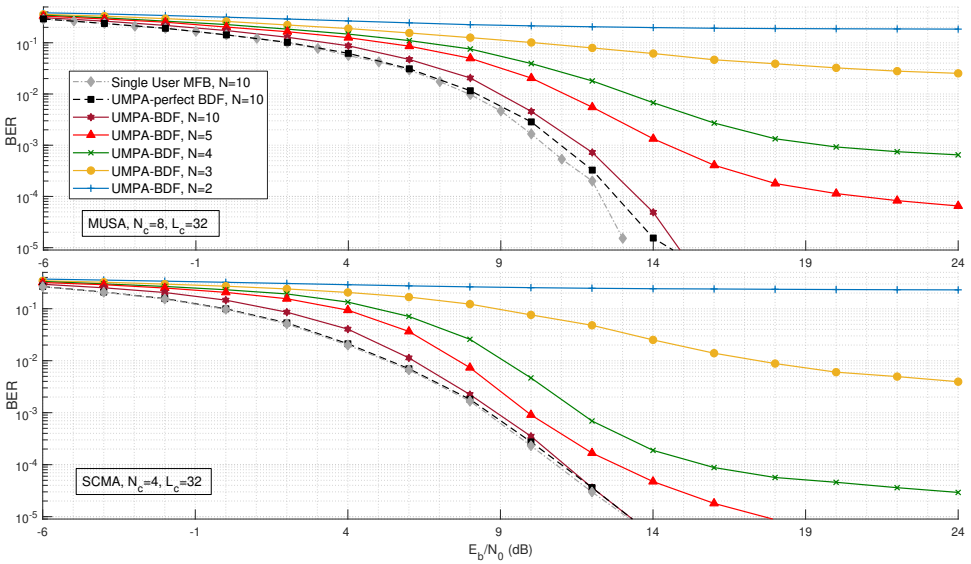

Figure 4.6: BER vs E_b/N_0 for MUSA ($N_c = 8, K = 12$) and SCMA ($N_c = 4, K = 6$) under 150% loading, $M = 16$, $L_c = 32$ $N = 1, 2, 3, 4, 5, 10$; Gaussian distributed tabs for MAC

have 150% overloading, but due to more MUI in MUSA, it is 0.5 dB away from the single user MFB while the SCMA sticks to it. Moreover, in $M = 16$ case to achieve the lower AIR bound, 5 antennas are required unlike SCMA which can reach the AIR bound with 4 antennas because it has less MUI only in this scenario. Therefore, the importance of the MUI can be understood more clearly from these BER and AIR results.

In Figure 4.8, the overloading is fixed to 250% via MUSA codes and the BER vs SNR performance of the UMPA-BDF is investigated in a dispersive channel with $L_c = 32$ by changing the code length to $N_c = 4, 8, 12$ and 16 which results in a different number of users for each scenario. From the figure, it can be seen that short codes bring better BER results when lower number of antennas are used (3 antenna results) at receiver since the number of users are less and therefore there is lower MUI at the receiver. However, as the number of antennas or RF chains increase the the performance difference is removed as the MUI is eliminated in the spatial domain during CMF operation by the antennas. Therefore, receiver performance is not affected by the code length and the number of users if adequate number of RF chains are provided. Furthermore, the required number of antennas is not increasing linearly with the number of users, which can be verified with $N_c = 16$ case where there are 40 users in MAC and only using 4 and 5 antennas is enough to achieve a

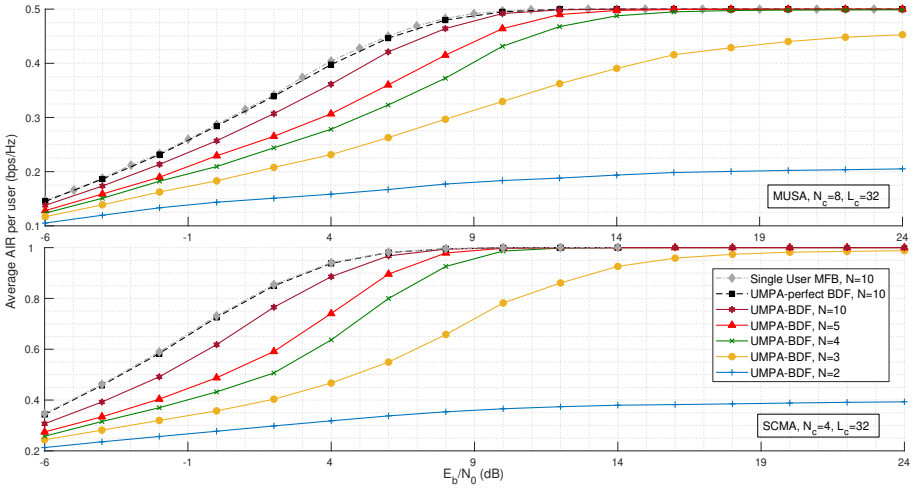

Figure 4.7: AIR vs E_b/N_0 for MUSA ($N_c = 8, K = 12$) and SCMA ($N_c = 4, K = 6$) under 150% loading, $M = 16$, $L_c = 32$ $N = 1, 2, 3, 4, 5, 10$; Gaussian distributed tabs for MAC

BER performance below 10^{-5} without using any outer channel coding. The same effect can be seen from $N_c = 12$ and $N_c = 8$ plots. These BER results can be verified with the AIR vs SNR curves in Figure 4.9. From the AIR plot, the maximum uncoded rate is achieved for 40 users in the $N_c = 16$ case by using only 4 antennas, and for 30 users in the $N_c = 12$ case having 3 antennas is adequate. One of the important result that can be drawn from Figure 4.8 and Figure 4.9 is that UMPA-BDF can support same loading for short and long N_c's by needing only 1 or 2 extra antennas.

After seeing the performance of the UMPA-BDF with 250% loading in MIMO-MAC, we have tried different loading conditions for variable code length for fixed E_b/N_0 value to see how many users can be accommodated with UMPA-BDF in MAC with very limited RF chains. In Figure 4.10, BER vs loading behavior of the MAC is investigated from 50% to 400% user overloading for $N_c = 4, 8, 12$, and 16. Using short code lengths with even 400% loading in $N_c = 4$ which corresponds to 16 users requires only 5 antennas while $N_c = 16$ under 400% loading corresponding to 64 users needs only 6 antennas to have the approximately same BER performance. With this graph, we can say that even under 400% loading no matter how many users are accommodated in MAC, 5 or 6 antennas are adequate to reduce MUI to a level that UMPA-BDF can handle. In addition ISI is equalized during the BDF operation in the receiver, so ISI is not a serious problem as long as the channels are perfectly known. Another important point is the flexibility of MUSA coding schemes which are differ-

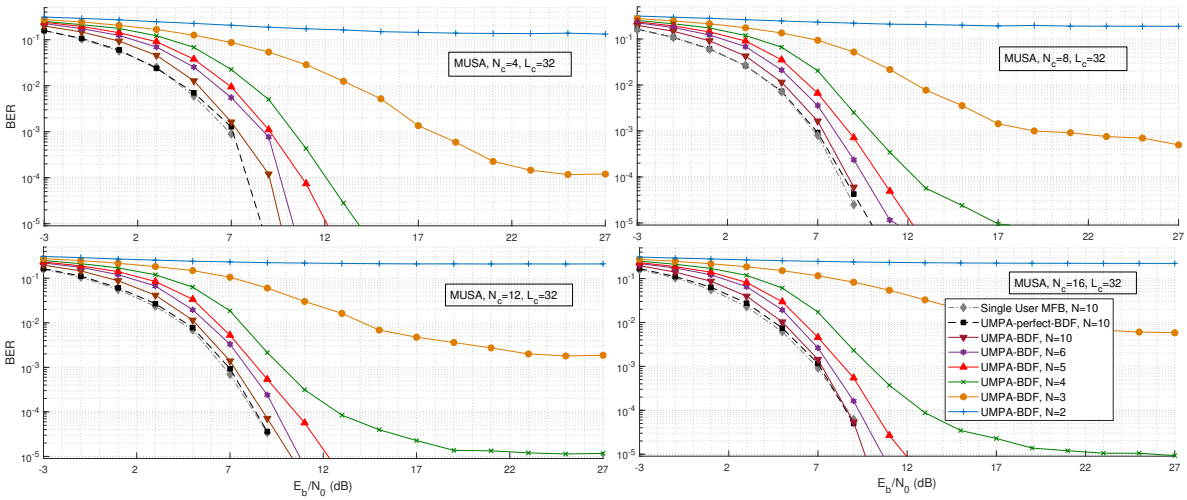

Figure 4.8: BER vs $\mathrm{E_b/N_0}$ for MUSA $N_c = 4, 8, 12, 16, K = 10, 20, 30, 40$ under 250% loading, $M = 4$, $L_c = 32$ $N = 2, 3, 4, 5, 6, 10$; Gaussian distributed tabs for MAC

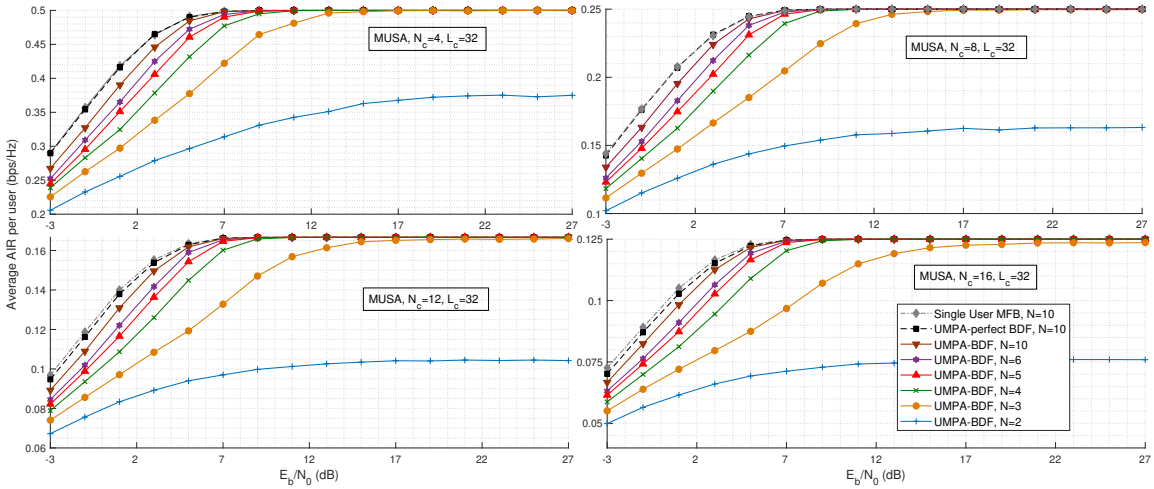

Figure 4.9: AIR (GMI) vs $\mathrm{E_b/N_0}$ for MUSA $N_c = 4, 8, 12, 16, K = 10, 20, 30, 40$ under 250% loading, $M = 4$, $L_c = 32$ $N = 2, 3, 4, 5, 6, 10$; Gaussian distributed tabs for MAC

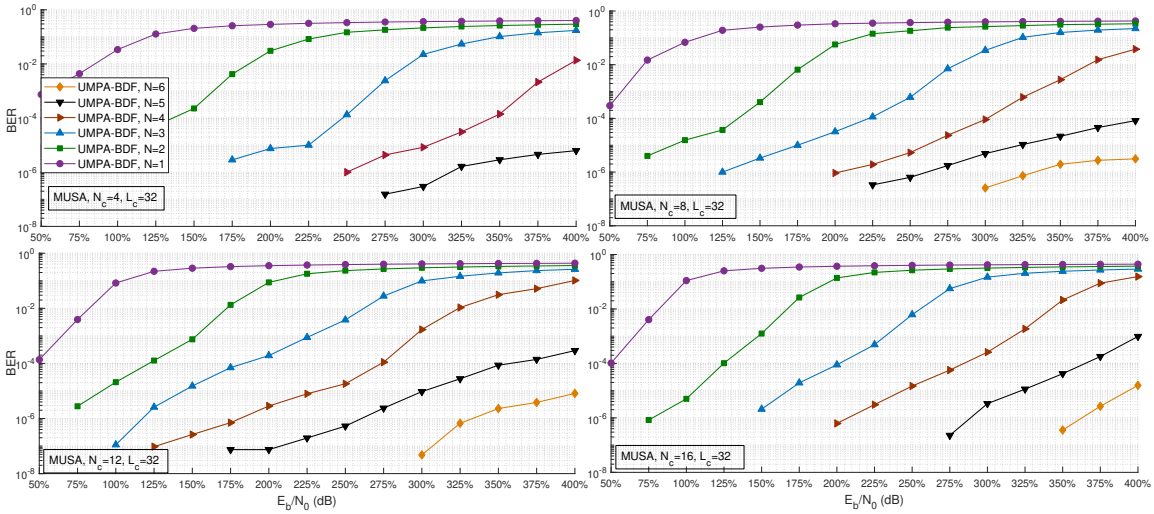

Figure 4.10: BER vs Loading, $E_b/N_0 = 22$ dB for MUSA $N_c = 4, 8, 12, 16$, $M = 4$, $L_c = 32$ $N = 1, 2, 3, 4, 5, 6$; Gaussian distributed tabs for MAC

ent than the SCMA sequences that requires a multi constellation and advanced codebook design techniques to provide more overloading. Using MUSA, we can freely change the overloading condition and make MUD under 400% loading with very few number of antennas. That is, the number of required antennas is not increasing with the number of users in MAC. In order to validate the results, AIR vs Loading curve of the same scenario can be seen in Figure 4.11. What we can see from this graph is in all N_c cases, using 5 antennas is enough to reach maximum uncoded data rate in the MAC, however if the less antennas were available it would be better choice to select short N_c's which has less number of users under high overloading conditions.

In Figure 4.12, the effect of L_c is investigated in order to show that ChDMA helps the receiver processing while separating the users. In this simulation, L_c is changed from 1 to 32 under 150% loading with constant $E_b/N_0 = 22$ dB. This results show that, CMF operation is really helpful for the receiver performance after $L_c = 4$ channel tabs as the BER drops down while increasing the L_c.

4.4.2 Narrowband Flat Fading Channels

In another simulation environment, assuming there is no interfering multipath components $L_c = 1$ with MUSA schemes, the BER and AIR with respect to E_b/N_0

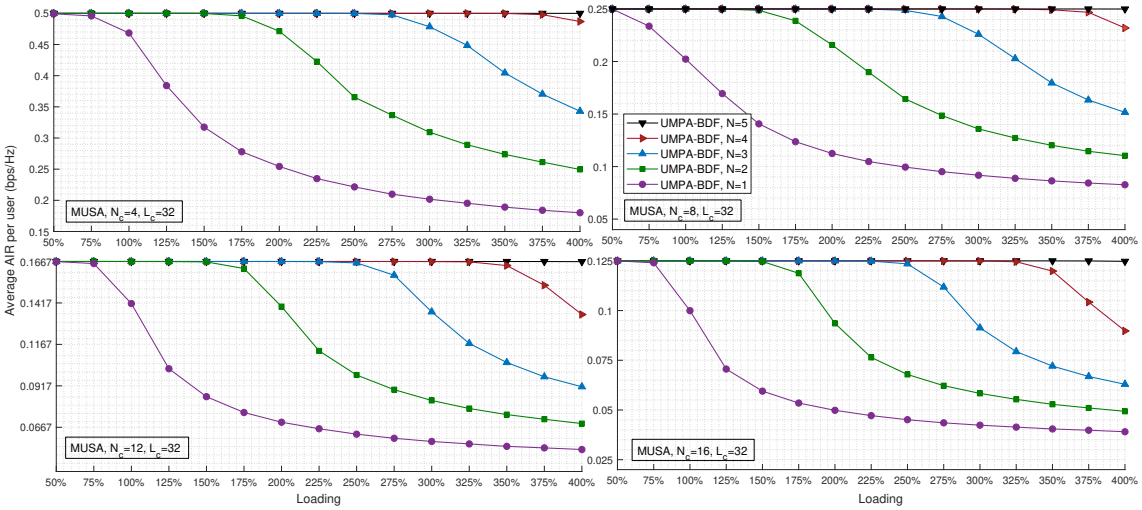

Figure 4.11: AIR vs Loading, $E_b/N_0 = 22$ dB for MUSA $N_c = 4, 8, 12, 16$, $M = 4$, $L_c = 32$ $N = 1, 2, 3, 4, 5, 6$; Gaussian distributed tabs for MAC

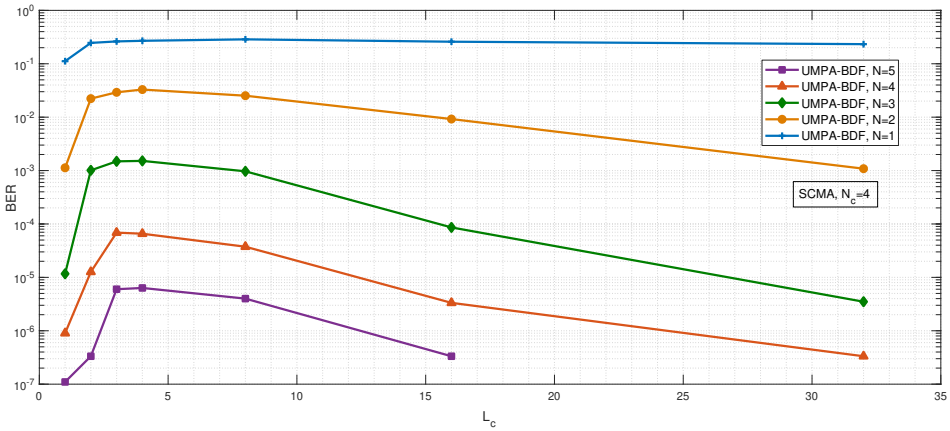

Figure 4.12: BER vs L_c for SCMA $(N_c = 4, K = 6)$ under 150% loading, $M = 4$, Gaussian distributed tabs for MAC

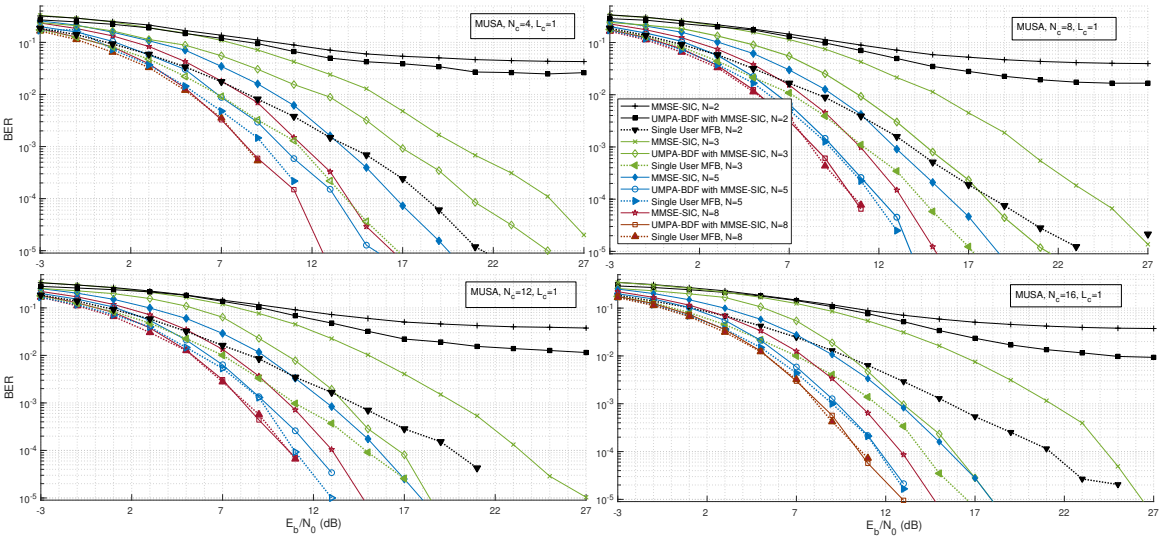

Figure 4.13: BER vs $\mathrm{E_b/N_0}$ for MUSA $N_c = 4, 8, 12, 16$, $K = 10, 20, 30, 40$ under $\%250$ loading, $M = 4$, $L_c = 1$ $N = 2, 3, 4, 5, 6, 10$; Gaussian distributed tabs for MAC

performance of the state-of-the-art MMSE-SIC receiver and UMPA-BDF algorithm whose first surviving path is constructed by the MMSE-SIC symbol estimates are shown together in Fig. 4.13 under 250% overloading for $N_c = 4, 8, 12$ and 16. The first iteration success of UMPA-BDF determines the BER performance significantly, therefore, using MMSE-SIC at the first iteration boost the UMPA-BDF performance and it reaches beyond MMSE-SIC BER success with up to 5 to 10 dB SNR gain. In this plot, for $N = 2, 3, 5, 8$ number of antennas MMSE-SIC results and MMSE-SIC aided BER performance is presented with the single user MFBs. The effect of UMPA-BDF improvement over MMSE-SIC can be best seen with the longer N_cs, particularly for $N_c = 16$. Examining the $N_c = 16$ with 40 users in $N = 3$ scenario approximately 9 dB SNR gain is obtained with the UMPA-BDF, and the similar improvements can also be seen from the other curves. Apart from this, despite the lack of L_c for user separation in CMF, using MMSE-SIC aided UMPA-BDF requires 4 antennas to superimpose the BER curves to the single user MFB except the $N_c = 4$ case which requires 5 antennas since the short codes have lower diversity among users. When investigating the corresponding AIR vs SNR plot in Figure 4.14, MMSE-SIC aided UMPA-BDF can reach the AIR bound with 3 antennas for all cases no matter what the N_c is.

Lastly, having seen the 250% loading performance of the MMSE-SIC aided UMPA-

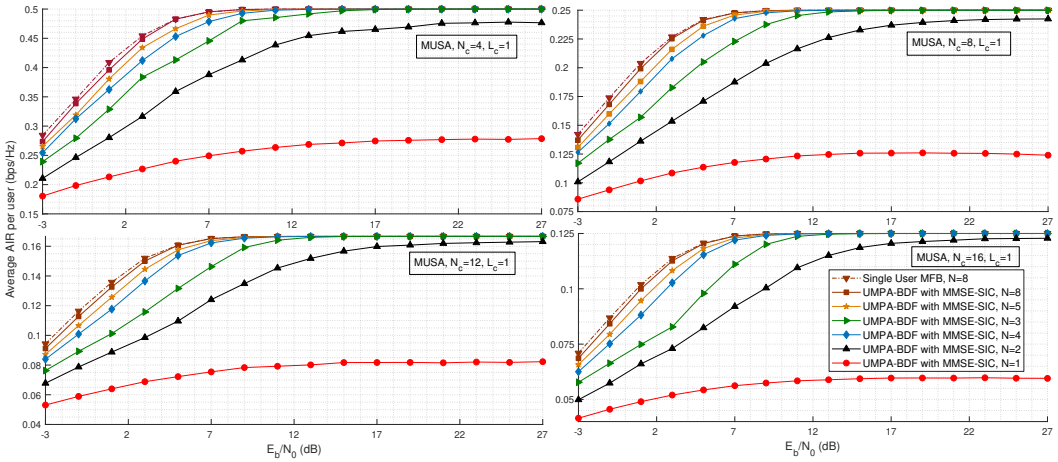

Figure 4.14: AIR vs $\mathrm{E_b/N_0}$ for MUSA $N_c = 4, 8, 12, 16, K = 10, 20, 30, 40$ under 250% loading, $M = 4$, $L_c = 1$ $N = 2, 3, 4, 5, 6, 10$; Gaussian distributed tabs for MAC

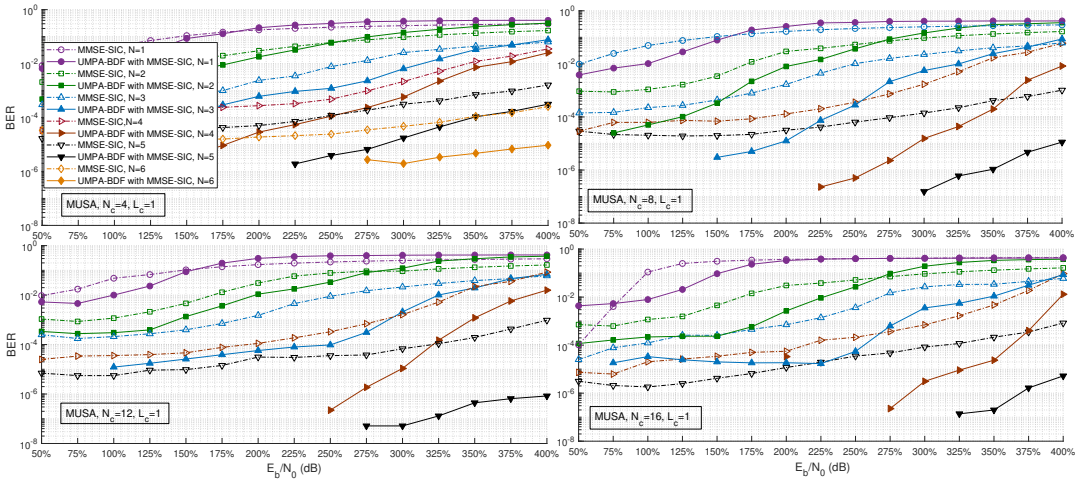

Figure 4.15: BER vs Loading, $\mathrm{E_b/N_0} = 17$ dB for MUSA $N_c = 4, 8, 12, 16$, $M = 4$, $L_c = 32$ $N = 1, 2, 3, 4, 5, 6$; Gaussian distributed tabs for MAC

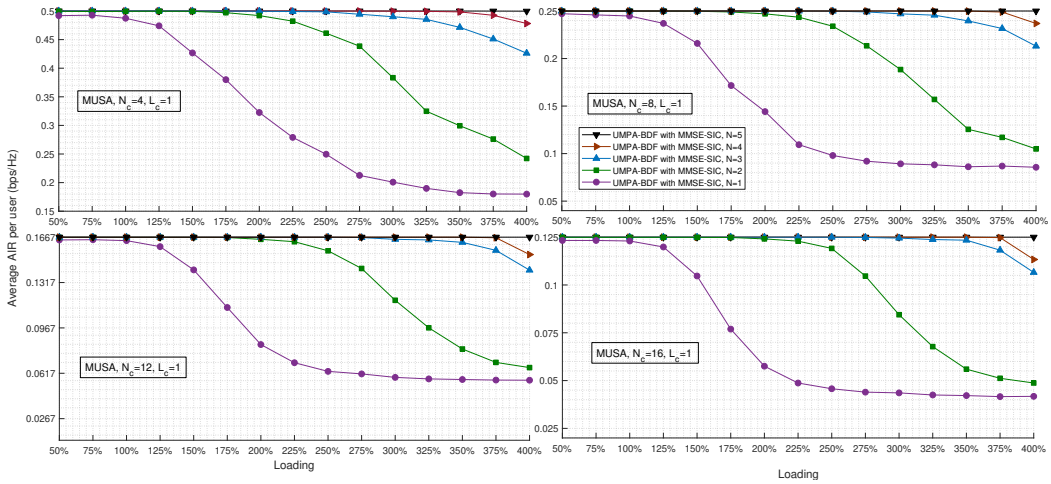

Figure 4.16: AIR vs Loading, $E_b/N_0 = 17$ dB for MUSA $N_c = 4, 8, 12, 16$, $M = 4$, $L_c = 32$ $N = 1, 2, 3, 4, 5, 6$; Gaussian distributed tabs for MAC

BDF under $L_c = 1$ fading channels, the uncoded BER vs Loading and AIR vs Loading performance of the same channel conditions for $N_c = 4, 8, 12, 16$ will be investigated in Figure 4.15 and Figure 4.16, respectively. Again we see that on the upper left part $N_c = 4$ need more antennas as it requires $N = 6$ while the longer N_cs reach the same performance with 5 antennas. This is because, the short N_c's have more correlation and bring less diversity to MMSE-SIC aided UMPA-BDF system. In this BER vs Loading comprasion, MMSE-SIC alone and MMSE-SIC aided UMPA-BDF performance can be directly compared.For $N = 1, 2$, although there is a performance improvement with MMSE-SIC aided UMPA-BDF as the loading increases BER performance is becoming worse as the number of antennas is not adequate to drive UMPA-BDF to eliminate the MUI. As for the $N = 3$ case, in all scenarios, there is a significant performance improvement up to $300\% - 350\%$ user overloading. However, when the number of antennas is above 3, MMSE-SIC aided UMPA-BDF receiver architecture has indisputable superiority over MMSE-SIC algorithm for all loading conditions. This is a very important results for the massive MIMO solutions where the beamforming allows only limited RF chains for the particular user group. In such cases, only assigning 5 antennas under 400% loading base station can still serve under 10^{-5} BER performance without any outer channel coding which is also removing the signaling cost. Having seen the BER comparison, in Figure 4.16, we can see the average AIR per user in the MAC for MMSE-SIC aided UMPA-BDF. It is clearly showing that using only $N = 5$ antennas allows the receiver to operate with

400% loading for $L_c = 1$ fading channels. Moreover, this performance is independent from the modulation type as it can be single-carrier or multi-carrier.

4.4.3 Higher Order Constellations with MUSA

In this simulation environment, we have $L_c = 8$ multipath fading channels where MUSA sequences are utilized to have higher order constellations in the NOMA MIMO MAC with 16 users. Since the computational complexity of UMPA-BDF algorithm grows linearly with the constellation size like the state-of-the art MMSE-SIC designs, increasing the constellation size does not cause complexity concerns. In this subsection we will investigate the UMPA-BDF receiver AIR performance from $M = 2$ to $M = 64$ in order to be able to see whether we can reach the maximum uncoded rate for the given conditions utilizing higher order QAM constellations. In Figure 4.17 and Figure 4.18, under 200% overloading by using 6 and 12 antennas at the receiver, AIR vs $\mathrm{E_s/N_0}$ curves are provided. From Figure 4.17, as the $\mathrm{E_s/N_0}$ increases it is safe to select $M = 16$ cardinality and after $\mathrm{E_s/N_0} = 21$ dB, system can support higher rates using $M = 32$ constellation even though it is not reaching the maximum uncoded rate. As for Figure 4.18 case, using 12 antennas, we are seeing that as the system can support $M = 64$ constellation size, it should be preferred in the communication scenario to have higher data rates. Provided figures are clearly showing that our proposed UMPA-BDF algorithm can work with higher order constellations depending on the operational SNR value and the number of antennas in the receiver. In other words, according to the average SNR value, integration of the adaptive modulation and suitable coding techniques with MUSA sequences, we can reach practical transmission rates which are close to ones given by AIR lower bounds in the Figure 4.17 and Figure 4.18

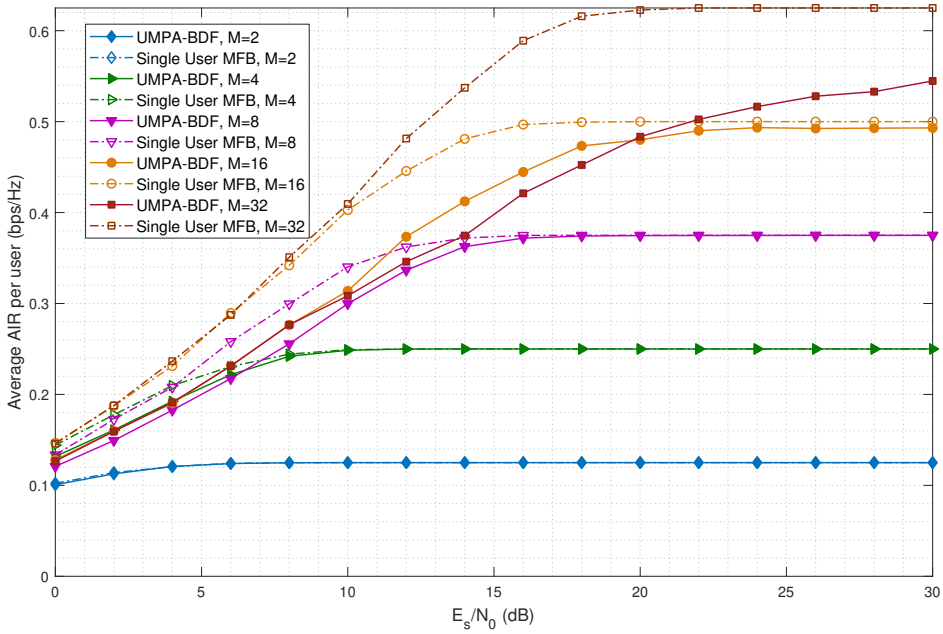

Figure 4.17: AIR vs E_s/N_0 dB for MUSA $N_c = 8$, $M = 2, 4, 8, 16, 32$, $L_c = 8$ $N = 6$, 200% Loading; Gaussian distributed tabs for MAC

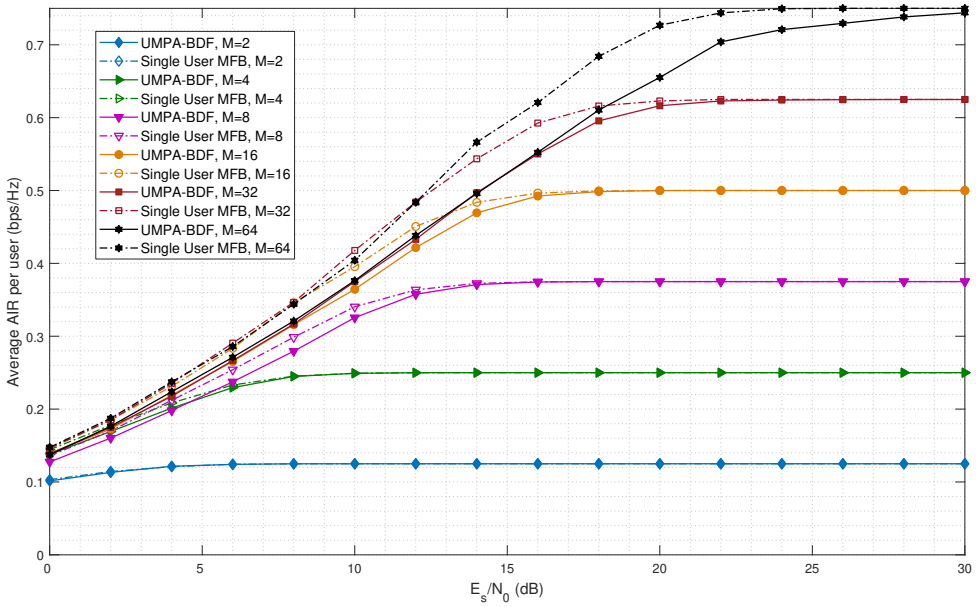

Figure 4.18: AIR vs E_s/N_0 dB for MUSA $N_c = 8$, $M = 2, 4, 8, 16, 32, 64$, $L_c = 8$ $N = 12$, 200% Loading;; Gaussian distributed tabs for MAC

CHAPTER 5

CONCLUSION

In this thesis, a generic low complexity iterative max-log MAP receiver which we call UMPA-BDF, is proposed for general MIMO NOMA MAC with code domain schemes. It realizes MUD at symbol rate via an efficient MPA, operating on Ungerboeck type FG where unwhitened MF outputs are directly utilized in highly dispersive channels. ChDMA is employed via CMFs in UMPA-BDF to mitigate the MUI at the received signal.

In order to implement the proposed receiver algorithm for this thesis work, first the discrete time equivalent of a general uplink MIMO NOMA MAC model has been derived using the channel and code correlations of the users. In this environment, the max-log MAP detection algorithm was carried out through the message passing for MUD in wideband dispersive gaussian channels, using the two exemplary code domain NOMA schemes which are SCMA and MUSA. Apart from these, state-of-the-art MMSE-SIC receiver algorithm was re-derived for MIMO compatible uplink NOMA channels. Utilizing the flexible MUSA coding scheme in flat fading MIMO channels, MMSE-SIC algorithm has been used to boost the performance of the UMPA-BDF. As a result, UMPA-BDF outperforms the state-of-the-art MMSE-SIC algorithm with lower receiver complexity. We have shown both wideband and narrowband applications of the UMPA-BDF algorithm with different coding schemes throughout this thesis in order to emphasize the generic architecture of the proposed algorithm which enables both single-carrier and multi-carrier modulation types for any coding type.

In the Numerical Evaluation part of this thesis, performances of the UMPA-BDF and MMSE-SIC aided UMPA-BDF algorithms in terms of BER and AIR lower bound

were presented for MUSA and SCMA schemes with respect to different operating SNR and overloading scenarios. Having carried out the simulations for different NOMA codeword lengths, number of antennas, and alphabet size, we have shown that even under high overloading conditions, by using only limited number of antenna elements/RF chains, and utilizing adaptive modulation techniques with suitable coding architecture, practical transmission rates, can be attained. Moreover, this practical rate values can be estimated by mismatched decoding capacity lower bound in Chapter 4 for different operating regimes.

From the loading curves given in Chapter 4, it can be inferred that MUSA based NOMA scheme with the use of UMPA-BDF receiver can be preferred in IoT applications, which require massive connectivity among multiple nodes, due to its flexibility in terms of number of served active users and NOMA codeword length. With this NOMA architecture, while arranging the NOMA codebook size of each user adaptively according to their power level, NOMA codeword lengths can also be changed adaptively as the number of users change in uplink MAC so that the system can meet the requirements for the increased user demand. The results for MUSA with codeword length $N_c = 16$ (where the connection of 64 users can be supported by using only 4 receiver antenna elements) show the effectiveness of the proposed architecture in applications requiring massive connectivity. Apart from these, it is safe to assume that the practical NOMA codewords are short enough to support the need of Ultra-Reliable Low Latency Communication (URLLC) type applications. In addition, required rate of the outer code, which can be integrated with NOMA scheme, can be determined via the mismatched decoding capacity lower bound according to the operating regimes (SNR and loading conditions), alphabet size (M), and the number of antennas (N) at the receiver side. Therefore, the NOMA parameters for MUSA are able to be reorganized for the different IoT modes with varying requirements.

At the end of this thesis work, the MATLAB codes and C based drivers in the form of dynamic link library (dll) of the proposed UMPA-BDF receiver algorithm are fully ready and in modular form. As future works, joint iterative channel estimation algorithm should be developed for the mobility scenarios, and the combination of the in-band full duplex methods with NOMA schemes might be considered utilizing the UMPA-BDF algorithm to increase the capacity of future wireless networks.

REFERENCES

[1] A. Goldsmith, *Wireless Communications*. Camridge University Press, 2005.

[2] Wikipedia. Wikipedia-code division multiple access. [Online]. Available: httpsen.wikipedia.orgwikiCode-division_multiple_access

[3] M. Vaezi, Z. Ding, and H. V. Poor, *Multiple Access Techniques for 5G Wireless Networks and Beyond*, 08 2018.

[4] L. Dai, B. Wang, Z. Ding, Z. Wang, S. Chen, and L. Hanzo, "A survey of non-orthogonal multiple access for 5g," *IEEE Commun. Surveys Tuts.*, vol. 20, no. 3, pp. 2294–2323, 2018.

[5] Y. Wu, C. Wang, Y. Chen, and A. Bayesteh, "Sparse code multiple access for 5g radio transmission," in *2017 IEEE 86th Vehicular Technology Conference (VTC-Fall)*, 2017, pp. 1–6.

[6] C. E. Rasmussen, "Factor graphs and message passing." [Online]. Available: http://mlg.eng.cam.ac.uk/teaching/4f13/1617/factorgraphs.pdf

[7] D. Tse and P. Viswanath, *Fundamentals of Wireless Communication*. USA: Cambridge University Press, 2005.

[8] L. Dai, B. Wang, Y. Yuan, S. Han, C. I, and Z. Wang, "Non-orthogonal multiple access for 5g: solutions, challenges, opportunities, and future research trends," *IEEE Commun. Mag.*, vol. 53, no. 9, pp. 74–81, Sep. 2015.

[9] Z. Ding, X. Lei, G. K. Karagiannidis, R. Schober, J. Yuan, and V. K. Bhargava, "A survey on non-orthogonal multiple access for 5g networks: Research challenges and future trends," *IEEE J. Sel. Areas Commun.*, vol. 35, no. 10, pp. 2181–2195, Oct 2017.

[10] M. Vaezi, Z. Ding, and H. V. Poor, *Multiple access techniques for 5G wireless networks and beyond*. Springer, 2019.

[11] W. Yuan, N. Wu, Q. Guo, Y. Li, C. Xing, and J. Kuang, "Iterative receivers for downlink mimo-scma: Message passing and distributed cooperative detection," *IEEE Trans. on Wireless Commun.*, vol. 17, no. 5, pp. 3444–3458, 2018.

[12] Y. Chi, L. Liu, G. Song, C. Yuen, Y. L. Guan, and Y. Li, "Practical mimo-noma: Low complexity and capacity-approaching solution," *IEEE Trans. Wireless Commun.*, vol. 17, no. 9, pp. 6251–6264, 2018.

[13] L. Liu, Y. Chi, C. Yuen, Y. L. Guan, and Y. Li, "Capacity-achieving mimo-noma: Iterative lmmse detection," *IEEE Transactions on Signal Processing*, vol. 67, no. 7, pp. 1758–1773, 2019.

[14] L. Liu, C. Yuen, Y. L. Guan, Y. Li, and C. Huang, "Gaussian message passing for overloaded massive mimo-noma," *IEEE Trans. Wireless Commun.*, vol. 18, no. 1, pp. 210–226, 2018.

[15] S. Tang, Z. Ma, M. Xiao, and L. Hao, "Performance analysis for mmwave mimo-scma systems using lens antenna array," in *2019 IEEE Int. Conf. Commun. Workshops (ICC Workshops)*, May 2019, pp. 1–5.

[16] L. Lu, G. Y. Li, A. L. Swindlehurst, A. Ashikhmin, and R. Zhang, "An overview of massive mimo: Benefits and challenges," *IEEE J. Sel. Topics Signal Process.*, vol. 8, no. 5, pp. 742–758, 2014.

[17] Z. Ding, X. Lei, G. K. Karagiannidis, R. Schober, J. Yuan, and V. K. Bhargava, "A survey on non-orthogonal multiple access for 5g networks: Research challenges and future trends," *IEEE Journal on Selected Areas in Communications*, vol. 35, no. 10, pp. 2181–2195, Oct 2017.

[18] R. Hoshyar, F. P. Wathan, and R. Tafazolli, "Novel low-density signature for synchronous cdma systems over awgn channel," *IEEE Transactions on Signal Processing*, vol. 56, no. 4, pp. 1616–1626, April 2008.

[19] R. Hoshyar, R. Razavi, and M. Al-Imari, "Lds-ofdm an efficient multiple access technique," in *2010 IEEE 71st Vehicular Technology Conference*, May 2010, pp. 1–5.

[20] H. Nikopour and H. Baligh, "Sparse code multiple access," in *2013 IEEE 24th Annual International Symposium on Personal, Indoor, and Mobile Radio Communications (PIMRC)*, Sep. 2013, pp. 332–336.

[21] X. Dai, S. Chen, S. Sun, S. Kang, Y. Wang, Z. Shen, and J. Xu, "Successive interference cancelation amenable multiple access (sama) for future wireless communications," in *2014 IEEE International Conference on Communication Systems*, Nov 2014, pp. 222–226.

[22] Z. Yuan, G. Yu, W. Li, Y. Yuan, X. Wang, and J. Xu, "Multi-user shared access for internet of things," in *2016 IEEE 83rd Veh. Technol. Conf. (VTC Spring)*, May 2016, pp. 1–5.

[23] R. H. Roy, "Spatial division multiple access technology and its application to wireless communication systems," in *1997 IEEE 47th Vehicular Technology Conference. Technology in Motion*, vol. 2, May 1997, pp. 730–734 vol.2.

[24] X. Dai, Z. Zhang, B. Bai, S. Chen, and S. Sun, "Pattern division multiple access: A new multiple access technology for 5g," *IEEE Wireless Communications*, vol. 25, no. 2, pp. 54–60, April 2018.

[25] M. Mohammadkarimi, M. A. Raza, and O. A. Dobre, "Signature-based nonorthogonal massive multiple access for future wireless networks: Uplink massive connectivity for machine-type communications," *IEEE Vehicular Technology Magazine*, vol. 13, no. 4, pp. 40–50, Dec 2018.

[26] Q. Xiong, C. Qian, B. Yu, and C. Sun, "Advanced noma scheme for 5g cellular network: Interleave-grid multiple access," in *2017 IEEE Globecom Workshops (GC Wkshps)*, Dec 2017, pp. 1–5.

[27] M. Taherzadeh, H. Nikopour, A. Bayesteh, and H. Baligh, "Scma codebook design," in *2014 IEEE 80th Vehicular Technology Conference (VTC2014-Fall)*, Sep. 2014, pp. 1–5.

[28] B. Wang, K. Wang, Z. Lu, T. Xie, and J. Quan, "Comparison study of non-orthogonal multiple access schemes for 5g," in *2015 IEEE International Symposium on Broadband Multimedia Systems and Broadcasting*, 2015, pp. 1–5.

[29] F. R. Kschischang, B. J. Frey, and H. . Loeliger, "Factor graphs and the sum-product algorithm," *IEEE Transactions on Information Theory*, vol. 47, no. 2, pp. 498–519, 2001.

[30] Jung-Fu Cheng and T. Ottosson, "Linearly approximated log-map algorithms for turbo decoding," in *VTC2000-Spring. 2000 IEEE 51st Vehicular Technology Conference Proceedings (Cat. No.00CH37026)*, vol. 3, May 2000, pp. 2252–2256 vol.3.

[31] G. M. Guvensen, Y. Tanik, and A. O. Yilmaz, "A novel transceiver architecture for highly dispersive noma channels," in *2018 IEEE 87th Vehicular Technology Conference (VTC Spring)*, June 2018, pp. 1–6.

[32] ——, "A reduced-state ungerboeck type map receiver with bidirectional decision feedback for m-ary quasi orthogonal signaling," *IEEE Transactions on Communications*, vol. 62, no. 2, pp. 552–566, 2014.

[33] G. Colavolpe and G. Germi, "On the application of factor graphs and the sum-product algorithm to ISI channels," *IEEE Trans. Commun.*, vol. 53, no. 5, pp. 818–825, May 2005.

[34] G. Colavolpe, D. Fertonani, and A. Piemontese, "Siso detection over linear channels with linear complexity in the number of interferers," *IEEE Journal of Selected Topics in Signal Processing*, vol. 5, no. 8, pp. 1475–1485, 2011.

[35] F. Kschischang, B. Frey, and H. Loeliger, "Factor graphs and the sum-product algorithm," *IEEE Trans. Inf. Theory*, vol. 47, no. 2, pp. 498–519, Feb. 2001.

[36] A. Hafeez and W. E. Stark, "Decision feedback sequence estimation for unwhitened isi channels with applications to multiuser detection," *IEEE Journal on Selected Areas in Communications*, vol. 16, no. 9, pp. 1785–1795, 1998.

[37] D. Tse and P. Viswanath, *Fundamentals of Wireless Communication*. Cambridge University Press, 2005.

[38] T. M. Cover and J. A. Thomas, *Elements of Information Theory (Wiley Series in Telecommunications and Signal Processing)*. USA: Wiley-Interscience, 2006.

[39] J. Scarlett, *Reliable Communication Under Mismatched Decoding*. University of Cambridge, 2014. [Online]. Available: https://books.google.com.tr/books?id=95_5vgEACAAJ

[40] J. Y. N. Hui, "Fundamental issues of multiple accessing," Ph.D. dissertation, Massachusetts Institute of Technology, Cambridge, MA, USA, 1983. [Online]. Available: http://hdl.handle.net/1721.1/15348

[41] G. Ungerboeck, "Channel coding with multilevel/phase signals," *IEEE Trans. Inf. Theory*, vol. 28, no. 1, pp. 55–67, Jan. 1982.

[42] N. Merhav, G. Kaplan, A. Lapidoth, and S. Shamai Shitz, "On information rates for mismatched decoders," *IEEE Transactions on Information Theory*, vol. 40, no. 6, pp. 1953–1967, 1994.

[43] A. Ganti, A. Lapidoth, and I. E. Telatar, "Mismatched decoding revisited: general alphabets, channels with memory, and the wide-band limit," *IEEE Transactions on Information Theory*, vol. 46, no. 7, pp. 2315–2328, 2000.

[44] A. Modenini, F. Rusek, and G. Colavolpe, "Optimal transmit filters for isi channels under channel shortening detection," *IEEE Transactions on Communications*, vol. 61, no. 12, pp. 4997–5005, 2013.

[45] M. Vameghestahbanati, I. D. Marsland, R. H. Gohary, and H. Yanikomeroglu, "Multidimensional constellations for uplink scma systems—a comparative study," *IEEE Communications Surveys Tutorials*, vol. 21, no. 3, pp. 2169–2194, thirdquarter 2019.